Marine Geology
August 2021, Volume 438 Pages 106524 (24p.)
https://doi.org/10.1016/j.margeo.2021.106524
https://archimer.ifremer.fr/doc/00709/82106/

Neogene to Quaternary evolution of carbonate and mixed carbonate-siliciclastic systems along New Caledonia's eastern margin (SW Pacific)

Tournadour Elsa [1, 2, *], Jorry Stephan [1], Etienne S. [2], Collot J [2], Patriat Martin [1], Boudagher-Fadel M. K. [3], Fournier F. [4], Pelletier B. [5], Le Roy Pascal [6], Jouet Gwenael [1], Maurizot P. [2]

[1] IFREMER, Unite Geosci Marines, F-29280 Plouzane, France.
[2] DIMENC, Serv Geol Nouvelle Caledonie, BP 465, Noumea 98845, New Caledonia.
[3] UCL, Earth Sci, 2 Taviton St, London WC1H 0BT, England.
[4] Aix Marseille Univ, Coll France, CEREGE, INRAE,IRD,CNRS, Case 67,3 Pl Victor Hugo, F-13331 Marseille 03, France.
[5] IRD, Geosci Azur UMR 6526, BP A5, Noumea 98800, New Caledonia.
[6] Univ Europeenne Bretagne Occidentale, IUEM CNRS, UMR Domaines Oceaniques 6538, Pl Copern, F-29280 Plouzane, France.

* Corresponding author : Elsa Tournadour, email address : elsa.tournadour@ifremer.fr

Abstract :

Neogene and Quaternary shallow-water carbonate records surrounding New Caledonia main island, Grande Terre, provide a good example for understanding the stratigraphic architecture of tropical mixed carbonate-siliciclastic systems. Due to a southeastern tilt of the eastern margin, the eastern shelf of Grande Terre has been better preserved from erosion than the western part, favouring the development and preservation of shallow-water carbonates. Based on the integration of bathymetric and seismic data, along with paleoenvironmental and biostratigraphic constraints derived from dredged carbonate rocks, a comprehensive geomorphological and architectural characterization of the offshore eastern margin of Grande Terre has been made. During the Mio-Pliocene, a wide, up to 750 m-thick carbonate build-up developed and extended over at least 350 km from north to south. This Mio-Pliocene build-up, currently lying at 300 to 600 m water depths, is overlain by a Pleistocene-Holocene barrier reef-lagoon complex and associated slope deposits. The switch from aggrading Neogene carbonate banks to backstepping Quaternary platforms likely reflects an increase in accommodation due to a high subsidence rate or to relative sea-level rise, and/or results from a switch in carbonate producers associated with global environmental changes. The internal architecture of the Quaternary barrier reef-lagoon complex is highlighted, especially the development of lowstand siliciclastic prisms alternating with transgressive shallow-water carbonate sequences. This pattern agrees with the reciprocal sedimentation model typically invoked for mixed sedimentary systems. This stratigraphic pattern is well developed in front of the Cap Bayes inlet in the north of our study area, yet it is not observed southward along the eastern margin. This difference suggests that other factors than relative sea-level variations directed the architecture of the margin, such as low terrigenous inputs, lagoon paleo-drainage networks or sediment by-pass towards deep basins.

Highlights

► An extensive Mio-Pliocene shallow-water carbonate bank lies at 300-600 m water depths around New Caledonia's main island. ► This bank evolved into Quaternary rimmed platforms due to regional subsidence and/or change in carbonate producers. ► Coeval terrigenous inputs with carbonate production are evidenced as early as the Serravalian. ► The architectures of mixed carbonate-siliciclastic systems vary widely alongshore, from north to south. ► Terrigenous inputs, paleo-drainage network or by-pass transport influenced the mixed system architectures.

Keywords : Mixed carbonate-siliciclastic system, Reciprocal sedimentation, Tropical carbonates, Terrigenous inputs, New Caledonia, SW Pacific

1. INTRODUCTION

Mixed carbonate-siliciclastic depositional systems are characterized by a high variability in facies and architectures resulting from several factors, such as relative sea-level change, tectonic motions, carbonate production, terrigenous inputs, sediment transfer and hydrodynamic conditions, complicating the sequence stratigraphy interpretation (Droxler and Jorry, 2013; Zeller et al., 2015). According to the classical "reciprocal sedimentation" model (Wilson, 1967), mixed systems in the tropical realm have been commonly subdivided into alternating temporal phases where siliciclastic deposits would prevail during low sea-level periods whereas carbonates would dominate during transgressions and highstands. This reciprocal concept is yet relevant for several ancient and some modern cases studies (Kerans & Tinker, 1999; Toomey et al., 2016), but has been shown to be inadequate in describing several others examples. This model appears not applicable for some mixed cool-water carbonate platforms, where sandstones can be deposited when wave abrasion depth rises above the seafloor during transgressions, whereas shell-beds formed during lowstands (Brachert et al., 2003). Another example is the Great Barrier Reef, where siliciclastic deposits are released to the slope and basin during late transgression, possibly due to the reworking of significant amounts of fine-grained terrigenous sediment stored on the shelf during lowstand (Wallace et al., 2002; Dunbar and Dickens, 2003; Mitchell et al., 2007; Harper et al., 2015). In addition, wave and/or current energy might prevent the infill of the lagoon during highstands, during which carbonate production is thought to be maximal, inducing, thus, an "empty bucket" pattern (Schlager, 1989; Purdy and Gischler, 2005; Zinke et al., 2001; Weij et al., 2019). This variability in the sedimentological response of mixed systems to relative sea-level changes demonstrates that other controlling parameters should also be considered in order to improve the prediction of their complex depositional architectures.

Around the main island of New Caledonia, "Grande Terre", Neogene to Quaternary shallow-water carbonate systems occur coeval with high terrigenous fluxes derived from the erosion of

rugged mountain ranges located all across the island and primarily composed of obduction-related thrust sheets. The oldest known Neogene shallow-water carbonates on Grande Terre are lower Miocene mixed carbonate-siliciclastic series cropping out in the Népoui area, on the western part of the island, close to the present day coastline (Fig. 1). These outcrops were interpreted as reflecting sediment deposition on Aquitanian and Burdigalian ramps where seagrass-related and scleractinian carbonate production occurred simultaneously to strong fluvio-deltaic terrigenous inputs (Maurizot et al., 2016; Tournadour et al., 2020). However, the offshore extent of this Miocene mixed system remains unknown.

At the present day, Grande Terre is surrounded by one of the largest modern barrier reef in the world. This barrier reef has been drilled on the western margin and past studies (Coudray, 1975; Cabioch et al., 2008b ; Montaggioni et al., 2011) showed that it initiated at 400 cal kyr B.P. or Marine Isotope Stage 11 (MIS 11), over non-reefal shallow water carbonates that were deposited as of *ca.* 1.2 Ma ago on a carbonate ramp or non-rimmed platform (Montaggioni et al., 2011). The inner lagoon, in turn, started its infill only since 200 cal kyr, B.P. or Marine Isotope Stage 7 (MIS7) (Le Roy et al., 2008). This points to the fact that the southwestern shelf of New Caledonia does not follow a classic reciprocal sedimentation pattern but constitutes a unique mixed carbonate-siliciclastic tropical system with a strong temporal and spatial partitioning between the outer coral plateau and the inner lagoon depression where terrigenous clastic sediments prevail (Le Roy et al., 2019).

In contrast, the Neogene to Quaternary shallow-water mixed systems of the eastern margin of Grande Terre are much less documented than their western counterparts, largely because of a lack of boreholes, rare outcrops onshore and few acoustic data offshore. However, this margin is thought to have a very different tectonic history than the western margin, probably a higher subsidence that would have resulted in a better preservation of shallow-water systems on the shelf, thus allowing to improve our understanding of the onset of Neogene carbonate systems and the transition to Quaternary barrier reef lagoon in the regional tectonic context. In addition, those sedimentary records allow to discuss the potential controlling factors determining the

stratigraphic architectures along the margin, such as terrigenous inputs or paleo-drainage networks. With that aim, we have compiled both existing and newly acquired geophysical data and dredged carbonate rock samples from Ponérihouen to Antigonia seamount (Fig. 1) to perform a comprehensive analysis of slope morphologies and to reconstruct the depositional environments and ages of the main terraces and seismic units observed along the eastern margin.

2. GENERAL SETTINGS

2.1. Geography

New Caledonia is a remote archipelago located in the South West Pacific (Fig.1). Its main island, Grande Terre, is a 50 to 80 km wide and approximatively 400 km long land stripe oriented in a N140° direction. Highest summits are *ca.* 1600 m high. Because of dominant southeastward trade winds (N110-120°) its eastern margin is positioned on the windward side, whereas the western margin is the leeward side. Its eastern part is typified by steep reliefs, deeply incised valleys and short coastal plains, whereas the western part has more extended valleys, wider alluvial lowlands and large coastal plains. This landform dissymmetry impacts the spatial distribution of rainfall, with the eastern windward coast receiving twice as much precipitation than the western leeward coast. Such differences induce a one-and-a-half-time higher river discharge along the eastern coast compared to the western coast (Terry & Wolting, 2011).

2.2. Tectonics

Grande Terre marks the northeastern tip of Zealandia (Mortimer et al., 2017), a mostly submerged fragment of continental crust isolated from Gondwana during the Late Cretaceous to Paleocene due to regional rifting followed by seafloor spreading in the Tasman Sea (Hayes & Ringis, 1973; Gaina et al., 1998). During the Eocene Grande Terre underwent a convergence

phase that led to the NE-SW emplacement of several tectonic nappes and finally, in the late Eocene-early Oligocene, to the obduction of a prominent kilometres-thick ophiolite mostly constituted of serpentinized peridotites (Paris, 1981; Maurizot et al., 2020). Once obduction terminated, extensional tectonics prevailed all over Grande Terre (Lagabrielle et al., 2005; Chardon & Chevillotte, 2006; Lagabrielle & Chauvet, 2008). During this post-obduction extensional phase, that may still be active today, widespread normal faulting affected both island margins. The assymetric morphology of Grande Terre is likely the result of these obduction and post-obduction tectonics. Drivers of the extension are either attributed to a plate tectonic divergent phase (i.e. far-field stresses related to initiation of east-verging subduction of the Australian plate beneath the Pacific Plate, Chardon & Chevilotte, 2006) and/or to post-orogenic collapse, dismantling and combined isostasic rebound (Lagabrielle et al. 2005, Lagabrielle & Chauvet, 2008; Moretti & Turcotte 1985; Collot et al., 2017). In this second hypothesis, unroofing the ridge of dense allochthonous mantle material and loading the adjacent basins resulted in subsidence of the basins and uplift of the ridge. The latter uplift is thus interpreted as being at the origin of the steepening of both the western and eastern margins of Grande Terre. The deep structure of the eastern margin has not been imaged by seismic data but is interpreted to be structured by a series of normal faults (see simplified geological cross-section of Fig. 1 and Collot et al. (1987)). Timing and amplitudes of these extensional events and vertical motions over the post-obduction period are not constrained as no continuous Oligocene to present day geological records exist. The Neogene to Quaternary carbonates that are the focus of this paper have developed on these structures. Offshore, towards the south, major listric normal faults bordering the obducted mantle sheets are imaged by seismic data along Pines Ridge (Chardon & Chevillotte, 2006; Flamand, 2006; Chardon et al., 2008; Patriat et al., 2018) (Fig.1). Apart from post-obduction extension, since the late Miocene, the southern part of Grande Terre and the Loyalty Islands are the foreland area of the Vanuatu Subduction Zone where the Australian Plate subducts beneath the Pacific Plate. A lithospheric flexure associated to this process is observed and results in the uplifts of the Loyalty Islands, the southern tip of Grande Terre and the Isles of

Pines. As a result, Quaternary 125 ka fringing reefs around Yaté and Isle of Pines are uplifted and now are positioned 10 to 20 m above present-day sea level (Cabioch et al., 1996).

2.3. Miocene mixed carbonate siliciclastic systems

On land, the post-obduction geology is characterized by an Oligocene sedimentary hiatus and the oldest known marine sediments that overlie allochthonous units are Miocene mixed carbonate-siliciclastic sedimentary rocks only cropping out in a restricted nearshore area located west of Grande Terre, in the region of Népoui (Coudray, 1975; Maurizot et al., 2016; Tournadour et al., 2020). These successions have been interpreted to reflect deposition of an Aquitanian carbonate ramp dominated by seagrass-related carbonate production, overlain by Burdigalian fan delta deposits that laterally evolve towards a carbonate ramp dominated by seagrass meadows and small-sized coral bioconstructions (Tournadour et al., 2020).

Offshore, despite a lack of drill core data, a few dredged carbonate samples were recovered from the outer slope of the eastern margin of Grande Terre (Chardon et al., 2008; Yamano et al., 2015) and close to *Munida* and *Crypthelia* seamounts (Daniel et al., 1976; Bitoun and Recy, 1982) (Fig. 2). These samples, collected between 400 m and 800 m water depths, are the only evidences of Miocene shallow-water carbonate deposits along the eastern margin of Grande Terre and Pines Ridge. Based on the interpretation of seismic profiles along Grande Terre's southeastern margin, Chardon et al. (2008) identified several normal faults that they interpret as being related to Late Miocene extensional tectonics. These authors also interpreted two planar surfaces as post-obduction erosional lateritic land surfaces resulting from weathering processes overlain by shallow-water carbonate deposits.

2.4. Quaternary carbonate systems

Our knowledge on the nature, structure and chronology of the New Caledonian Quaternary carbonate systems primarily comes from coring investigations carried out through the western parts of the New Caledonian barrier system (Coudray, 1976, Cabioch et al., 2008b;

Montaggioni et al., 2011). Four cores, 120 to 226 m-long, reached the upper Cretaceous and Eocene bedrock and allowed to characterize the Quaternary development history of the western carbonate shelf margin. The recovered carbonate sequences result from stacking of about ten sedimentary carbonate units that were deposited during successive transgressive and high sea-level stands corresponding to interglacial periods (Cabioch et al., 2008b). These units are separated from each other by unconformities formed during sea-level drops in glacial periods. The succession of depositional events was reconstructed using lithostratigraphy, magnetostratigraphy, uranium-series dating and nannofossil stratigraphy (Cabioch et al., 2008b; Montaggioni et al., 2011). Carbonate sediment production was initiated prior to 1.2 Ma within an open shallow-water shelf margin, which acted as a carbonate ramp system until 0.48 Ma. Corresponding deposits forming the lower units recovered in boreholes (red dots on Fig. 1) include grainstone, packstone and wackstone rich in corals, coralline algae, encrusting foraminifera with locally thick rodoliths accumulations (Montaggioni et al., 2011). The ramp system is assumed to have evolved into a rimmed, reef platform as of 0.40 Ma. The initiation of coral reef tracts and the associated reef-rimmed platform are thus considered to have begun after MIS 11 (Montaggioni et al., 2011), i.e. the Mid-Brunhes Event. Corresponding sedimentary units are made up of stacked *poritid*-rich framework beds correlated to reef-flat environments with moderate to lower-water energy, and coralgal frameworks partly including arborescent acroporids suggesting deposition in a protected reef-flat setting (Montagggioni et al., 2011). Complementary studies of the Quaternary evolution of the south-west lagoon obtained seismic, bathymetric and coring data (Le Roy et al., 2008; Le Roy et al., 2019). Results showed that infill is composed of two or three 100 ka sedimentary sequences with a first significant flooding of the lagoon assumed to have started during MIS7, at 220 cal kyr B.P. The disparate ages of the lagoon and reefs can be reconciled with the fact that the first reefs were probably initially fringing structures without a significant lagoon that has expanded later in response to subsidence of the margin and reef growth (Le Roy et al., 2018). Offshore, the outer barrier reef slopes of Grande Terre are marked by five marine terraces located between ca. 20 and ca. 120 m water depths

198 that Flamand (2006) tentatively correlated to the five reefal lithological sequences cored on the
199 western barrier reef and interpreted as the morphological expressions of Quaternary
200 interglacials. However, a younger, last deglacial origin for these terraces located above 120 m
201 water depth cannot be ruled out. Note that these Quaternary marine terraces are located in the
202 area indicated by the blue arrow on bathymetrical and seismic data (Figs. 5 to 8).

203 *2.5. Quaternary subsidence rates*

204 Based on cores of the Quaternary barrier reef of the western margin of Grande Terre, subsidence
205 rates are estimated to range between 0.03 to 0.20 mm.yr^{-1} since the last 400 ka (Coudray, 1975;
206 Cabioch et al., 1996; Flamand, 2006; Frank et al., 2006) and display mean rates of ≤0.08 mm.yr^{-1}
207 over the past 1 Ma (Montaggioni et al., 2011). Such values possibly reflect a long-term
208 subsidence of the western margin of Grande Terre suggesting that post-obduction extensional
209 tectonics are still active and allowing sufficient accommodation space to record most Quaternary
210 sea-level highstands. Unfortunately, the lack of core data on the eastern margin does not allow
211 reconstructing any Neogene to Quaternary vertical motions.

212 3. DATA AND METHODS

213 Our morphological and stratigraphic analyses are based on the integration of existing and
214 newly acquired bathymetrical and 2D seismic reflection data supplemented by dredged rock
215 samples (Fig. 2). Existing bathymetrical data are derived from four datasets. The former covers
216 the lagoon of Grande Terre and was essentially acquired during hydrographic surveys of the
217 French Navy (SHOM), compiled by the New Caledonia Government within a 25 m resolution
218 grid. The second dataset corresponds to data acquired between 2002 and 2006 onboard RV *Alis*
219 (EM1002 multibeam echosounder) along all the outer slopes of Grande Terre and Loyalty
220 islands, as well as on seamounts of the Pines Ridges (down to *ca.* 1000 m of water depth), in the
221 framework of the ZoNéCo program (*e.g.* Pelletier et al., 2002, 2004, 2012; Perrier et al., 2004a,
222 2004b, 2004c, 2005) and IRD research projects (*e.g.* Cabioch et al., 2002a, 2002b). The third

223 dataset consists of data acquired in the 90's and 2000's in deeper waters (>1000 m of water
224 depth), such as in the South Loyalty Basin, onboard RV *L'Atalante* (EM12D multibeam
225 echosounder), again through ZoNéCo (*eg.* ZoNéCo-1, Pautot et al., 1993; ZoNéCo-2, Lafoy et al.,
226 1994; and ZoNéCo-3; Missègue et al., 1996). These two multibeam datasets were compiled in
227 2009 in 25 m (EM1002) and 100 m (EM12D) resolution grids by New Caledonia Government
228 (Juffroy, 2009) and included in the 2012 atlas of New Caledonia (Pelletier et al., 2012). The
229 fourth dataset is the global seafloor topography derived from satellite altimetry and ship depth
230 soundings (Smith and Sandwell, 1997). Newly acquired bathymetrical data corresponds to those
231 gathered by the KANACONO cruise onboard R/V *Alis* (Puillandre & Samadi, 2016).

232 The seismic dataset mainly consists of published multichannel seismic reflection profiles
233 located on the upper slope of the eastern margin of Grande Terre, acquired onboard R/V *Alis*
234 during the NEOMARGES cruise (Chardon et al., 2007), using a 24 channel streamer and a 20
235 cubic-inch air gun source. The high-resolution images have a maximum penetration of 0.25 s two
236 way time (twt) (Table 1) and were reinterpreted in this study through detailed line drawings.
237 Seismic profiles 206-04 (Lafoy et al. 1998) and AUS-104 (Bitoun & Recy et al. 1982), which are
238 publicly available in the *Tasman Frontier seismic database* (Sutherland et al., 2012), were also
239 interpreted. These profiles were acquired using lower frequency seismic devices (see Table 1)
240 and hence have a lower resolution but a higher penetration, reaching 3 s twt in the offshore
241 basins. Seismic stratigraphic analysis was performed on these profiles including identification of
242 seismic facies, unconformities and sequences following Mitchum et al. (1977). To estimate the
243 thickness of the carbonate units on the Pines Ridge, we assumed that they are composed of
244 shallow-water carbonates with a low-porosity, affected by early compaction and dissolution, for
245 which we attributed a mean velocity of 3000 $m.s^{-1}$ (Anselmetti & Eberli, 2001).

246 Sedimentary facies determinations were made on 17 carbonate rock samples dredged
247 during the DR-2005-NC and KANACONO cruises onboard R/V *Alis* (Pelletier et al., 2006;
248 Puillandre & Samadi, 2016; respectively) in water depths between 250 and 900 m (Table 2).
249 Samples were described from large thin sections in order to identify textures and main

components and ultimately reconstruct depositional environments. Biostratigraphic datings and paleoenvironmental reconstructions were based on the interpretation of foraminiferal assemblages (larger benthic and planktonic foraminifera). In our definitions of stratigraphic ranges, the planktonic foraminiferal zonal scheme of BouDagher-Fadel (2015, 2018a) is used. This scheme is tied to the time scale of Gradstein et al. (2012) and the revision by Cohen et al. (2017).

4. PHYSIOGRAPHY, STRUCTURE AND STRATIGRAPHY OF THE EASTERN MARGIN

4.1. Lagoon

The eastern lagoon, extending from the shoreline to the external barrier reef, is 10-15 km wide between Poindimié and Yaté with an average water depth of 40 m, whereas the western lagoon does not exceed a width of 5-10 km with an average water depth of 20 m, except in its southern part where it is deeper and wider (Le Roy et al., 2008, 2019). Another difference with the western lagoon, which is bounded by continuous barrier reefs, is that the eastern lagoon is typified by a discontinuous external barrier reef with drowned segments in its southern part, off Yaté (Cabioch et al., 1996; Andrefouet et al., 2009) (Fig. 2). The eastern lagoon can be divided into three morphological domains: (1) the shallow-water coastal zone, (2) the median lagoon and (3) the external barrier reef (Fig. 3B).

The shallow-water coastal zone is particularly well-developed between Ponérihouen to Thio, where coastal bays are shallow and have gentle slopes, due to terrigenous deltas located at river and estuarine mouths (Fig.3). The deltaic deposits extend for 2.5 to 7 km and can reach the central part of the lagoon. Between Côte Oubliée and Yaté, deltas are very restricted and do not exceed 2 km in length (Fig.3A). Previous studies on unconsolidated seafloor sediments revealed that these deltas are mainly composed of terrigenous sediments (Chevillon, 1997).

The deeper median lagoon, is relatively flat in its central part and contains isolated patch reefs as well as sandy islets aligned parallel to the coastline (Fig.3A). Southeast of the East Ngoé Pass, the median lagoon deepens (with an average water depth of 60-70 m) and contains a meandering channel that runs parallel to the coastline (Fig. 3A). This channel extends over 30 km, incises the lagoon up to 40 m deep and is connected to the Kouakoué Pass, where it runs perpendicular to the coastline thanks to a *ca.* 90° bend (Fig.3A).

The barrier reef domain comprises the reef crest, close to sea level, as well as a back-reef and reef flats within a 5 km-wide shallow-water area (20 to 40 m water depths). The latter is dominated by carbonate sediments of heterogeneous grain size, ranging from fine-grained sands to gravels (Chevillon, 1997). The barrier reef domain is interrupted by numerous passes (ie. inlets) connected to lagoonal channels that cross-cut the back-reef domain and are oriented roughly perpendicular to the coastline and the reef crest (Fig.3).

4.2. Outer slope

4.2.1 Overall slope profile

The outer slope morphologies of Grande Terre were previously described by Bitoun and Récy (1982), Rigolot (1989), Flamand (2006) and Pelletier et al. (2012). The outer slope of the western margin is very steep with values up to 20° between 0 to 2000 m water depths. This margin is very abrupt as the upper part of the slope is also very steep (see W-01 and W-02 profiles Fig.4). In comparison, the outer slope of the eastern margin, from Poindimié to Yaté, is smoother and extends over 15 to 20 km from the platform edge to the toe of slope at a water depth of approximately 2200 m (Fig. 4). It is composed of 3 domains: (1) the upper slope, characterized by a slope gradient lower than 3°, between 100 to approximately 500 m water depths and extending up to 20 km in areas preserved from the erosion (*e.g.* offshore Côte Oubliée and Yaté, see E-01 profile Fig.4). On the contrary, some areas are devoid of an upper slope domain and canyon heads are in direct contact with the external barrier reef (e.g. offshore

299 Houaïlou, see E-02 profile Fig.4); (2) the middle slope shows a slope gradient of up to 10°
300 between 400-500 m to approximately 2200 m water depth; (3) the lower slope and toe-of-slope
301 domain shows a gentle slope gradient ranging from 0.5 to 1°. This slope section starts
302 approximately at 2200 m water depth, which corresponds with the transition to the Loyalty
303 Basin floor. The slope section contains numerous erosional by-pass features such as submarine
304 canyons that incise the slope up to a depth of 200 m. Backscatter imagery reveals depositional
305 lobes at canyon mouths, offshore Thio and Yaté, as previously reported by Cotillon et al. (1989,
306 1990). The cut off angles are intended to characterize the morphology of the slope and have no
307 universal value. Even in the case of a Gaussian slope angle evolution (*sensu* Adams and Kenter,
308 2013) angle values may vary between different carbonate systems.

309 ***4.2.2 Physiography of the upper slope***

310 The upper slope is delimited by a major scarp located at 300-400 m water depth close to
311 the Cap Bayes Pass (Fig. 5A) and the Nakéti Pass (Fig. 6A), at 400-500 m water depth in front of
312 Côte Oubliée (Fig. 7A) and at 500-600 m water depths close to the Yaté Pass. The low-angle
313 upper slope is only 3 to 4 km wide close to Nakéti Pass and widens southward to reach a width
314 of 20 km in the vicinity of Yaté (Fig. 3A). Arcuate scars occur along the scarp, suggesting slope
315 failure processes along the upper slope (Fig.5A and 6A). In front of Côte Oubliée, the 5-6 km
316 wide upper slope is incised by low sinuosity, U-shaped, 40 to 80 m deep gullies (Fig.7A). Gullies
317 are of variable extension along the upper slope, some start at 150 m water depth close to the
318 outer reef slope, whereas others, shorter, gullies start at 300 m water depth, 3-4 km away from
319 the shelf edge. The majority of gullies are located in front of Kouakoué Pass through which they
320 are connected to the meandering lagoonal channel (Fig.3A).

321 ***4.2.3 Stratigraphy of the upper slope***

322 Seismic profiles covering the platform edge to the upper slope region reveal two main
323 seismic units, U1 and U2 separated by unconformity S1 (Fig. 5, 6 and 7). These profiles also
324 show that U1 is exposed on the seafloor along a major scarp (see red arrows on maps and

profiles of Fig. 5, 6 and 7). U1 comprises wavy reflections and is delimited at its top by erosional truncations and toplap terminations at bounding surface S1. The latter is overlain by unit 2 (U2) which shows well-layered reflections downlapping onto S1 (Figs. 5, 6 and 7). The maximal thickness of U2 varies between 0.1 to 0.25 s twt. In front of Côte Oubliée, on profile NM-13, at the mouth of the Kouakoué Pass, U2 is twice as thick than on profile NM-12b located 20 km further north at distance from any pass (Fig. 7).

Seismic profile NM1 at the mouth of the Cap Bayes Pass displays a well-developed unit U2 which forms a 0.2-0.25 s twt thick sedimentary prism (Fig. 5) composed of five stratigraphic sequences each composed of retrogradational sets (in pink on Fig. 5) overlain by progradational clinoform foresets (in beige on Fig. 5), noted 1 to 5. The slope break of the youngest (5^{th}) clinoform foreset (annotated "Clinoform slope break" on Fig. 5) is located at 150 m water depth. Retrogradational sets contain low-amplitude, mound-shaped seismic reflections that are only observed in topsets. Progradational sets show high-amplitude sigmoidal oblique reflections that downlap onto the underlying unit and are mainly located in the distal part of the sedimentary prism.

4.3. Pines Ridge

The Pines Ridge corresponds to the structural extension of the eastern margin of Grande Terre towards the South (Fig. 2). It is a NNW-SSE trending structure extending from the Isle of Pines to the Cook Fracture Zone.

4.3.1 Basement structure and first-order seismic stratigraphy of the Pines Ridge

The Pines Ridge is a horst of peridotite bounded by normal faults (Bitoun & Recy, 1982; Patriat et al., 2018) and is the southern offshore extension of the Peridotite Nappe cropping out onland (Patriat et al., 2018). In this paper, we have studied the area comprised between the Isle of Pines and Antigonia seamount, where Pines Ridge is the shallowest (Fig. 8A). Seismic profile

AUS-104 (Fig. 8B) reveals that the Pines Ridge comprises at its top high-amplitude subparallel reflections between 0.7 and 0.9 s twt, which contrast with the transparent seismic character of the underlying acoustic basement. Along the eastern flank of the Pines Ridge, the acoustic basement crops out on the seafloor at 2000 m water depth and was sampled by dredge GEO-I-3D (Daniel et al., 1976; Bitoun & Recy, 1982) (Fig. 8). The samples comprised altered basalt pebbles within a carbonate mud matrix containing planktonic foraminifera from the late Oligocene – earliest Miocene (Daniel et al., 1976). At that location, the acoustic basement forms a slightly tilted plateau located between 2.5 and 2.7 s twt, interpreted as an erosional weathering surface on top of peridotites by Bitoun and Recy (1982). This peridotite platform constitutes the western edge of the South Loyalty Basin (Figs. 8B and 8C). The peridotite basement is covered by a seismic unit composed of discontinuous low-amplitude subparallel reflections that is about 0.2 s twt thick at the crest of the ridge and up to 0.6 s twt-thick on its eastern flank. This unit is interpreted as a post-obduction sedimentary sequence (Bitoun & Recy, 1982 ; Patriat et al., 2018). The unit is incised by several submarine canyons along the eastern slope that extend from the Pines Ridge to the South Loyalty Basin (Fig. 8).

4.3.2 Physiography of the Pines Ridge

Along the northern part of the Pines Ridge, on the upper slope, the terrace identified on the eastern outer slopes of Grande Terre is continuously present between 300 to 600 m water depths (red arrows on Fig. 8A). East of the Isle of Pines, this terrace is affected by arcuate scarps most likely corresponding to submarine gravity collapses. Towards the Antigonia seamount, the top of the Pines Ridge is capped by this terrace (Fig. 2). Indeed, between the Banc de la Torche and Antigonia seamounts, the ridge's top remains positioned at 400-500 m water depth and its eastern slope is again characterized by a steep gradient and collapse features (red arrows on Fig. 8A). In turn, the Banc de la Torche and Antigonia display flat tops in 30 m to 60 m water depths (blue arrows on Fig. 8A). These two submerged isolated banks are surrounded by two terraces at 80-90 m and 120 m water depth.

The isolated Crypthelia and Munida seamounts are delimited by a main scarp at 400-500 m water depths (Figs.2 and 8). Their tops are located at 194 m and 93 m water depths, respectively. The Crypthelia seamount is 3 km wide and 12 km long elongated in a N160° direction (Fig. 9A and 9B). Three fault scarps located approximatively in 250, 350 and 500 m water depth affect the seamount across its entire length. Fault scarp heights are comprised between 30 m and 100 m (see map and cross section of Fig. 9B). In the northern part, the eastern fault scarp is associated with a channel probably formed by bottom currents circulating along the footwall of the fault (Fig. 9A and 9B). The southern edge of the seamount is marked by two 2-3 km wide failure scars, evidenced by arcuate headscarps located between 350 to 600 m water depth. The Munida seamount, located further to the northeast, extends over 8 km wide and 18 km long with a N60° direction (Fig. 9C). Its edges are bordered by N60° and N160° oriented fractures. On its southern flank, a terrace (M1) bordered by fault scarps is identified between 400 m and 600 m water depth. Above 200 m water depth, the top of the seamount (M2) is relatively flat (Fig. 9C) but still shows terraces at 100 m and 120-130 m water depth.

4.3.3 Stratigraphy of the Pines Ridge

The internal architecture of the post-obduction sedimentary sequence overlying basement of Pines Ridge and Munida seamount are imaged by seismic profile 206-04 (Fig.10). Over the Pines Ridge, the capping sedimentary unit reaches up to 0.5 s twt thick, i.e. approximately 750 m thick considering a velocity of 3000 $m.s^{-1}$ for a 30% porosity limestones according to Geldart (2004). In details, this interval is composed of 3 units, UP1 to UP3 (Fig.10C and 10D). Unit UP1 mainly developed on the SW edge of the ridge and is composed of low-amplitude reflections northeastwardly downlapping on basement. Unit UP2 downlaps basement on the eastern edge of the ridge with very low-amplitude reflections that form mounded morphologies. To the west, the seismic character of UP2 laterally evolves into low-amplitude, wavy to horizontal parallel reflections onlapping onto UP1 towards the southwest. Unit UP3 is typified by low-amplitude, sub-parallel and nearly horizontal reflections with low relief, mounded morphologies on the eastern edge of the ridge. Because seismic line 206-04 runs along

the south-eastern slope of Munida Seamount (Fig. 9C), seismic imaging is poor due to 3D lateral effects. However, the profile intersects a part of the seamount with less slope that reveals that the sedimentary sequence has a minimum thickness of 0.4 s twt, i.e. approximately 600 m-thick (Fig.10A and 10B). It is composed of two distinct seismic units, UM1 and UM2 (Fig.10). Unit UM1 overlies the basement and comprises low-amplitude subparallel mounded reflections with downlapping and onlapping terminations. Unit UM2 overlies UM1 and comprises high-amplitude subparallel reflections with downlapping terminations.

4.4. Lithologies and biostratigraphic ages

4.4.1 Eastern margin of Grande Terre

Seven carbonate rock samples have been collected along the upper slope of the eastern margin (Table 3, see location on Fig. 2). DR44 and DR45 were recovered on scarps located at 400 m and 600 m water depths, at the seafloor exposure of seismic unit U1 (see location on Figs. 6A and 6B). DR44 is a micritic packstone with recrystallised algae, large benthic foraminifera (LBF) of Serravallian age (PZ N12, Tf2, 13.82 Ma to 12.00 Ma) (see BouDagher-Fadel, 2018b) and corals. These elements are reworked within a pelagic mud dominated by plancktonic foraminifera (Table 4) that comprise *Globigerinoides quadrilobatus* (Fig.11A, b.), *Dentoglobigerina altispira* (Fig.11B, b.), *Globorotalia menardii* (Fig.11B, c.), *Globigerinoides conglobatus* (Fig.11B, d.), *Globigerinoides ruber* (Fig.11B, e.), *Truncorotalia crassaformis*, *Orbulina universa, Globorotalia plesiotumida* (Fig.11C, a), *Sphaeroidinella dehiscens* of Early Pliocene age (N19-N20a, 5.3 Ma to 3.6 Ma). DR45 comprises ultramafic pebbles and gravels encrusted by algae incorporated in a micritic packstone similar to that of DR44 and also includes *Lepidocyclina* sp. (Fig. 11D) and *Alveolinella praequoyi*, with the same Serravallian age. DR46, DR47 and DR48 were collected on the edge of the terrace located between 200 to 400 m water depths near the Nakéti Pass (Figs. 6A and 6C). These three samples consist of micritic wackestone/packstones with patches of reworked pelagic micritic facies. DR46 assemblages are dominated by planktonic foraminifera such as *Truncorotalia crassaformis* (Fig, 11E, a.) *T.*

truncatulinoides, *Globorotalia inflata, Globorotalia menardii* and *Orbulina univesa* of Pleistocene age (N22, 1.8 Ma to 0.12 Ma). DR47 sample shows numerous terrigenous grains (quartz, altered serpentine and undifferentiated clasts). Planktonic foraminifera are common and include *Globoquadrina dehiscens* (Fig. 11F, a.), *Globigerinoides quadrilobatus, Globigerinoides trilobus, Globigerinoides ruber, Globorotalia tumida, Globigerinoides spp.*, and *Pulleniatina obliquiloculata* of Late Pliocene age (N20a, 3.8 Ma to 3.6 Ma). DR48 contains numerous recrystallized algae and reworked LBF, such as *Alveolinella praequoyi* (Fig. 12A, a.) of Serravallian age (see Adams, 1984; BouDagher-Fadel and Banner, 1999; BouDagher-Fadel, 2018b), planktonic foraminifera of Pleistocene in age (N22, 1.8 Ma to 0.12 Ma) such as *Pulleniatina obliquiloculata* (Fig. 12A, b.), *P. primalis* and *Neogloboquadrina dutertrei*. DR49 sample was collected along the scarp at 500 m water depth, near the East Ngoé pass. The lower part of this scarp corresponds to the top of seismic unit U1 (Table 3, see location Figs.7A and 7B). Recovered samples comprise a micritic packstone with algae and LBF of Serravallian age, such as *Alveolinella praequoyi* (Fig. 12B, a.) and planktonic foraminifera such as, *Globorotalia tumida* (Fig12C, a.), *Sphaeroidinellopsis subdehiscens*, *Globorotalia menardii* and *Globorotalia inflata* of Early Pliocene age (N19b, 4.2 Ma to 3.8 Ma) after BouDagher-Fadel (2018a). DR53 is located further south, in front of the Yaté Pass, in ca. 280 m water depth, and is a micritic packstone containing planktonic foraminifera such as *Pulleniatina primalis* (Fig.12D, a.), *Prosphaeroidinella parkerae, Pulleniatina praecursor, Globigerinoides obliquus* and *Truncorotalia crassaformis* of Late Miocene to Early Pliocene age (Table 3, see location Fig.2).

4.4.2 Pines Ridge

Seven carbonate rocks were sampled along the Pines Ridge (Table 3, see location Fig. 2 and Fig.8A). These samples are mainly micritic wackestones/packstones with planktonic foraminifera and algae. Samples DW4737-B, DW4745-B, DW4746-B, DW4747-B1 and DW4747-X have ages ranging from Pliocene to Late Pleistocene (N19 to N22, 5.33 Ma to 0.12 Ma). Planktonic foraminifera assemblages of these samples include *Neogloboquadrina pachyderma, Sphaeroidinella dehiscens, Truncorotalia truncatulinoides, Truncorotalia tosaensis,* and

Pulleniatina obliquiloculata and LBF, such as *Alanlordia* sp. (Fig.12E, a.), are found reworked together with Pliocene planktonic foraminifera into the younger assemblages. Further south, samples DW4757-A and DW4782-A were collected along the eastern slope of Pines Ridge (Table 3, see location Fig.8A and Fig.10). DW4757-A includes Oligocene to earliest middle Miocene LBF such as *Lepidocyclina* sp. and *Planorbulinella solida* (Fig.12F, a.), while DW4782-A comprises late Miocene to Pleistocene (N17-N20, 8.6 Ma to 3.4 Ma) planktonic foraminifera such as *Neogloboquadrina humerosa, Sphaeroidinellopsis seminulina, Sphaeroidinellopsis subdehiscens*.

4.4.3 Munida seamount

Three carbonate rock samples have been collected along the edges of *Munida* (Table 3, see location on Fig. 8A and Fig. 9C). Samples from DW4770, located on the northeast flank of the seamount, comprise micritic and sparitic packstones composed of algae and planktonic foraminifera, such as *Truncorotalia truncatulinoides* (Fig.12F, a) and *Truncorotalia tosaensis* (Fig.12F, b) of Pleistocene age (N22, 1.8 Ma to 0.12 Ma). DR4772-A and DR4773-A samples, located on the southern flank, are grainstones cemented by sparite, with planktonic foraminiferal assemblages including *Sphaeroidinellopsis subdehiscens*, *Sphaeroidinella dehiscens, Truncorotalia tosaensis* and *Pulleniatina obliquiloculata* of Pliocene to Pleistocene age (N21-N22, 3.4 Ma to 0.12 Ma). These samples also reveal many reworked Miocene and Pliocene planktonic foraminifera.

4.5. Paleoenvironmental interpretations

The assemblages of DR44 and DR45 are dominated by Early Pliocene planktonic foraminiferal assemblages (e.g. *Sphaeroidinellopsis paenedehiscens, Globoquadrina dediscens, Orbulina universa, Globorotalia plesiotumida, G. tumida* and *Dentoglogigerina altispira*). These mixed, globular and heavily keeled planktonic foraminifera are indicative of inner to outer neritic environments (BouDagher-Fadel, 2015). Miocene larger benthic foraminifera (e.g. *Lepidocyclina* sp., *Katacycloclypeus martini*, *Cycloclypeus* sp.) and fragments of corals and rodophyte species are also frequently reworked within the deeper Early Pliocene platform. These larger benthic foraminifera are flat in shape and are associated with symbiont-bearing diatoms (Leutenegger 1984; Romero et al. 2002). They are common in forereef environment where they adapted to light attenuation with increasing habitat depth (Hottinger, 1983; Hallock and Schlager, 1986; Hohenegger, 1995; 2005; Yordanova & Hohenegger, 2002; 2007; BouDagher-Fadel, 2018b).

The Late Pliocene to Pleistocene deposits of DR46, DR47 and DR48 contain mainly planktonic foraminifera of mixed assemblages of globular forms (e.g. *Globigerinoides quadrilobatus, Orbulina universa*) and keeled globorotalids (e.g. *Truncorotalia truncatulinoides, Globorotolia tumida).* These assemblages are indicative of an inner to outer neritic environment (see BouDagher-Fadel, 2015). Micritic patches of older Miocene deposits with mainly globular small globigerinids (e.g. *Catapsydrax cf. dissimilis, Globigerina praebulloides*) are also present indicating the reworking of an inner neritic Miocene platform within the deeper deposits of the Pliocene.

DR 49 is interpreted as being deposited in an Early Pliocene inner to outer neritic platform. It contains planktonic foraminifera assemblages dominated by globular forms (e.g. *Globorotalia menardii, G. inflata, Globigerinoides trilobus, Glides quadrilobatus)* with occasional occurrences of keeled forms (e.g., *Globorotalia tumida, G. menardii*) and thickly coated forms in a thick, smooth cortex of calcite, *Sphaeroidinerlla dehiscens.* The latter is an extant thermocline dweller found rarely in subsurface, tropical, and subtropical waters (Chaisson and Ravelo, 1997; BouDagher-Fadel, 2018b). Reworked reefal Miocene larger benthic foraminifera (e.g., *Alveolinella praequoyi, Lepidocyclina sp., Planorbulina larvata, Amphistegina lessonii, Operculinoides spp., Gypsina sp*.) are also present. The presence of the large fusiform miliolid, *A. praequoyi* indicates the reworking of shallow reefal facies into the deeper Early Pliocene neritic environments.

The assemblages of DR53 are dominated by Late Miocene to Early Pliocene globular planktonic foraminifera species (e.g., *Neogloboquadrina pachyderma, N. acostaensis, Orbulina universa, Prosphaeroidinella parkerae, Pulleniatina praecursor, P. primalis, Globigerinoides obliquus*). Occasional keeled forms (e.g., *Truncorotalia crassaformis, Globorotalia menardii, Globorotalia tumida*) are also present. Larger benthic foraminifera such as *Amphistegina spp*. and *Sphaerogypsina spp.* are also found. The extant *Amphistegina* has adapted to high energy conditions, however, it is also found in mud free sands in areas of sea grass or coralline algae and in reefal areas down to depths of 35m (McKee et al, 1959), while *Sphaerogypsina* is generally common in shallow-water reefal environments (Nebelsick et al. 2001). These assemblages are interpreted as being deposited in an inner to outer neritic platform.

All samples from Pines Ridge point to inner to outer neritic settings, except DW4757-A which is typified by a forereef environment because of the occurrence of larger benthic foraminifera, such as *Amphistegina lessonii, Lepidocyclina sp., and Planorbulinella solida.* All samples from Munida seamount contain mixed assemblages of globular and keeled planktonic foraminifera (e.g., *Sphaeroidinellopsis subdehiscens, Sphaeroidinella dehiscens, Truncorotalia tosaensis, Pulleniatina obliquiloculata, Globorotalia inflata*) and are thought to reflect inner to outer neritic settings.

5. CARBONATE SYSTEM EVOLUTION ON THE EASTERN MARGIN OF NEW CALEDONIA

5.1 Mio-Pliocene carbonate banks

Carbonate rocks sampled on the upper slope scarp along the eastern margin contain algae, benthic foraminifera and coral fragments evidencing shallow-water carbonate production as early as the middle Miocene (Serravalian) and up to the Pliocene (Table 3, Fig. 13). This scarp corresponds to the top of seismic unit U1, which is bounded by the gently downslope dipping surface S1 (Figs. 5, 6 and 7). Because of its planar character, Chardon et al., (2008) interpreted this surface, topping a clastic continental wedge, as a lateritic land surface formed by weathering during emersion. Because none of the dredges that sampled this scarp (and thus U1) contained any traces of lateritic deposits, we propose an alternative interpretation where seismic unit U1 corresponds to a Mio-Pliocene carbonate bank, presently located at 300-600 m water depth. This important subsidence cannot be explained only by eustatism and we suggest that the post-obduction normal faulting that affected the Peridotite Nappe is likely the main driver of the subsidence. Surface S1 is interpreted as the top of the carbonate bank characterized by low-inclination features (Fig. 13A and B). The numerous ultrabasic pebbles/gravels and quartz grains within the carbonate matrix of samples DR45 and DR47 suggest coeval siliciclastic input

541 with the carbonate buildup development. A similar mixed carbonate-siliciclastic system also
542 occurs along the coastal domain of the western margin of Grande Terre in the well-constrained
543 Burdigalian Népoui system (Tournadour et al., 2020) (Fig.13B). The onset of these mixed
544 systems indicates that both margins of Grande Terre experienced shallow marine conditions
545 during the Miocene. However, their current positions, up to 20 m above present day sea level for
546 the Lower Miocene Népoui outcrops of the western margin and up to 500 m water depth for the
547 middle Miocene samples of the eastern margin, suggest a contrasted tectonic evolution of the
548 margins.

549 Our results suggest that the Mio-Pliocene carbonate platform (Table 3, Fig.13) extended
550 southward along the Pines Ridge, over peridotite horsts, which were at that time located in
551 shallow-water (Fig.13A and B). Within this sedimentary succession, unit UP1 is interpreted as an
552 attached carbonate platform developing on the western edge of the ridge. The eastward
553 thickening of unit UP2, which unconformably overlies unit UP1 (Fig.10D), suggests deposition
554 simultaneous or subsequent to the eastward tectonic tilting of Pines Ridge. The aggrading
555 mounded reflections of the lower part of UP2 on the eastern edge of the ridge, may be
556 interpreted as shallow-water, reefal bioconstructions (e.g. Miocene from the Browse basin,
557 Australia: Belde et al., 2017), or as an oligo-mesophotic bank with dominant algal and
558 foraminiferal production (e.g. Lower Miocene from Myanmar: Teillet et al., 2020a and 2020b).
559 However, in the upper part of UP2, the upward change from mounded to flat-topped
560 morphologies on the eastern margin strongly suggests the development of reef-flat
561 environments aggrading up to sea-level. Finally, subunit UP3 is also characterized by a slight
562 overgrowth along the eastern edge as evidenced by low-relief mounded reflectors (Fig.10). Such
563 an asymmetric feature could be explained by the continuation of an eastward tectonic tilt or
564 could be related to eastward winds driving carbonate growth (Fig.10).

565 Based on seismic interpretation, two stages of carbonate growth are identified on the
566 Munida seamount (seismic units UM1 and UM2). A carbonate sample, collected 15 km away
567 from the seamount (GEO-I-13D; location on Fig.2), contains benthic foraminifera indicative of

568 shallow-water environment, that can be dated Early Miocene (Daniel et al., 1976; Bitoun and
569 Recy, 1982). This sample suggests a first stage of carbonate growth (UM1) of Miocene age coeval
570 with carbonate platforms from Pines Ridge (UP1 and/or UP2) (Fig.13A and B). A Miocene
571 carbonate platform also likely developed on the Crypthelia seamount as suggested by a Middle
572 to Late Miocene carbonate sample exhibiting forereef facies (GEO-I-9D, see location Fig.2 and
573 Fig.9A) (Daniel et al., 1976; Bitoun and Recy, 1982).

574 Based on aforementioned observations, we propose the following palaeogeographical
575 reconstruction of the distribution of Mio-Pliocene shallow-water carbonate systems along the
576 margin of New Caledonia (Fig. 13B). The Mio-Pliocene carbonate systems extend for about 350
577 km, along the southeastern margin to Antigonia Seamount. On the western margin, the
578 Quaternary carbonate reef-lagoon system directly overlies Eocene allochthonous units (see
579 Fig.1). At that location, the absence of Miocene shallow-water deposits could be explained by a
580 non-deposition or by erosion in relation to the uplift of the western margin. The thickness of the
581 Miocene ramp is a least 200 m on the Nepoui area (Maurizot et al., 2016; Tournadour et al.,
582 2020), but remains unknown along the eastern margin. However, it can be estimated to be
583 around 750 m on the Pines Ridge (Fig.10B). Similar Miocene carbonate growth rates have been
584 reported for the southwestern Pacific suggesting that, in addition to local tectonic control
585 (subsidence) allowing significant volumes of sediments to accumulate, larger-scale
586 oceanographic or global factors favoured a sufficiently high carbonate production to fill the
587 created accommodation. For example, the 600 m-thick Marion Plateau platforms, northeast of
588 Australia, result from robust carbonate growth through early and middle Miocene up to its
589 terminal demise in the late Miocene (Ehrenberg et al., 2008). Along the northwestern shelf of
590 Australia, seismic profiles reveal a giant middle Miocene prograding barrier reef that
591 backstepped in the late Miocene (McCaffrey et al., 2020). Finally, the Gulf of Papua is also
592 structured by large-scale isolated long-lived carbonate platforms during the late Oligocene-early
593 Miocene and which demised during late Miocene-early Pliocene (Tcherepanov et al., 2008b). In
594 our study, the prolific Mio-Pliocene carbonate accumulation is favoured by the subsidence of the

595 shelves of New Caledonia and Pines Ridge, most likely in relation to post-obduction extensional
596 tectonics (Lagabrielle and Chauvet, 2008; Patriat et al., 2018).

597 *5.2 Transition from Mio-Pliocene to Quaternary platforms*

598 Along the eastern margin of Grande Terre, the Quaternary rimmed platform is thought to
599 have backstepped onto a Mio-Pliocene carbonate bank (Fig. 13A and 13C). Southward, along the
600 Pines Ridge and associated seamounts, the Mio-Pliocene carbonate banks are drowned but
601 several Quaternary flat-topped isolated platforms survived and aggraded.

602 In the vicinity of the study area, the carbonate platform of Maré, on the Loyalty Ridge,
603 records a significant change in the nature of carbonate production which is rhodalgal-dominated
604 during the late Miocene, and coralgal-dominated during the Pliocene (McNeill and Pisera, 2010;
605 Maurizot et al., 2020). These authors explain the switch of carbonate production by the trend of
606 decreased coralline red algae species richness (Aguirre et al., 2000) combined with the global-
607 scale Zanclean Flood Event (McKenzie et al., 1999). The exposure of these carbonate records
608 would result from the local tectonic uplift of the Loyalty Ridge related to Pliocene-Pleistocene
609 lithospheric flexure associated with the New Hebrides subduction (Dubois et al., 1974 and
610 1975).

611 Along the western margin of Grande Terre, the coral reef flourished from 400 ky (MIS-
612 11) considered as a period of luxuriant reef expansion in the southwest Pacific (Cabioch et al.,
613 2008b). Nevertheless, during the Quaternary, non-reefal carbonates were identified prior to
614 MIS-11 as early as 1.4 Ma, overlapping the Eocene allochtonous units and could form the
615 foundation of the Quaternary rimmed platform (Cabioch et al., 2008b; Montaggioni et al., 2011).

616 Along the eastern margin, the occurrence of a Mio-Pliocene platform below the eastern
617 barrier reef-lagoon suggests that an older carbonate platform developed similarly to what is
618 observed in Maré Island. The common occurrence of normal faults suggests that the eastern
619 margin and Pines Ridge were dominated by tectonic subsidence that would have promoted

accommodation for Neogene carbonate deposition and preservation, by opposition to the western margin where the Quaternary carbonates are found on top of Eocene peridotites. However, high subsidence rates could also explain the demise of the Mio-Pliocene carbonate systems along the Pines Ridge and the backstepping of Quaternary platforms. After 125 ky, the southeastern margin is slightly uplifted in the Yaté area and the Isle of Pines (Launay, 1985; Cabioch et al., 1996). This uplift could be due to the isostatic rebound of the central part of Grande Terre (Cabioch et al., 1996; Lagabrielle and Chauvet, 2008) or alternatively, could be associated with the lithospheric bulge of the New Hebrides subduction which is known to have a regional impact from the Loyalty Islands to the Isle of Pines (Dubois et al., 1974 and 1975; Cabioch et al., 1996). Hence, both margins of New Caledonia seem to have been affected by long-term subsidence during the Quaternary which, together with high-amplitude eustatic sea-level variations, allowed the aggradation and preservation of the reef-lagoon successions.

5.3 Quaternary carbonate platform

5.3.1 Late Quaternary mixed carbonate siliciclastic systems along the eastern margin

At the mouth of the Cap Bayes Pass, seismic unit U2 forms a 200 m-thick prism comprising five stratigraphic sequences (Fig. 5). In detail, the internal geometries of these parasequences are characterized by successive sets of aggrading to retrograding mounded reflections and progradational inclined reflections. We interpret these parasequences as mixed carbonate-siliciclastic prims that developed at the mouth of the pass, with aggrading and retrograding shallow-water carbonate sequences that developed during a transgression (pink colour on Fig. 5C), deposited during the last glacial-interglacial Quaternary cycles. This interpretation is consistent with core data collected on the western barrier reef (see location of Fig. 1), which revealed that the barrier reef itself consist of four to five lithological sequences deposited during successive transgressions and highstands in sea level since the Mid-Brunhes, each transgressive reefal units being separated by subaerial unconformities (subaerial

646 exposures) (Cabioch et al., 2008b; Montaggioni et al., 2011). The prograding seismic patterns
647 (yellow colour on Fig.5C) thus can be interpreted as lowstand siliciclastic wedges that formed
648 during Late Quaternary glacial lowstands.

649 Siliciclastics might have developed contemporaneously with the Quaternary barrier reef
650 bordering the eastern lagoon (Figs. 5, 6B and 7). This observation is consistent with the
651 reciprocal sedimentation concept traditionally developed for carbonate-siliciclastic mixed
652 systems (see review by Chiarella et al., 2017). According to this concept, siliciclastic deposits
653 prevailed on the upper slope during sea-level lowstands and at the beginning of the shelf
654 reflooding, whereas carbonate facies dominate during transgressions and highstand periods.
655 This configuration is currently observed on the platform edge of Quaternary mixed carbonate-
656 siliciclastic systems such as the Australia and Papua New Guinea Reef (Tcherepanov et al.,
657 2008a; 2008b; 2010; Harper et al., 2015; Mallarino et al., 2021) or the Belize Barrier Reef (Esker
658 et al., 1998; Ferro et al., 1999; Gischler et al., 2010; Droxler and Jorry, 2013). However, the
659 reciprocal pattern is not expressed everywhere along the upper slope of the eastern margin.
660 Near the Côte Oubliée, seismic unit U2 is not characterized by sedimentary prograding
661 clinoforms but rather by a downlapping aggrading wedge with a maximum thickness of 200 m in
662 front of the Kouakoué Pass (Fig.7). The lack of prograding features associated with the lowstand
663 clastic wedge could be explained by low terrigenous sedimentation rates as suggested by small
664 deltas restricted to the coastal domain (Fig. 3A). Moreover, the southeastern part of the lagoon is
665 characterized by a meandering channel network parallel to the coast and to the barrier reef,
666 suggesting an alongshore transport which can partly intercept outgoing sedimentary flux from
667 lagoon (Fig. 3A). In addition, the numerous gullies cutting the upper slope suggest high off-bank
668 sediment transport toward the deep basin and thus the accumulation of sediments along the
669 upper slope (Fig. 7A). This off-bank sediment transport could result from density cascading
670 processes driven by seasonal meteorological conditions (Wilson and Roberts, 1992, 1995). The
671 alongslope heterogeneity of the eastern margin upper slope deposits clearly shows that the
672 behaviour of a mixed carbonate-siliciclastic margin is difficult to predict and is not only

673 dependent of relative sea-level changes, as mentioned previously (Chiarella et al., 2017;
674 O'Connell et al., 2020).

675 ### *5.3.2 Quaternary isolated flat-topped banks of Pines Ridge and seamounts*

676 Along the Pines Ridge, dredged carbonate rock samples show that shallow-water
677 carbonate deposition occurred on the Banc de la Torche and Antigonia seamounts during the
678 Quaternary (Fig.13A and C). The two marine terraces at 80-90 m and 120 m water depth might
679 evidence reef backstepping during the last deglacial sea-level rise, as reported around the Great
680 Barrier Reef (Webster et al., 2018), the Gulf of Mexico (Khanna et al. 2017), the Maldives
681 (Fürstenau et al., 2010; Rovere et al., 2018), the SW Indian Ocean (Jorry et al., 2016), the
682 Marquesas Island (Cabioch et al., 2008a) and in Tahiti (Camoin et al., 2012). Carbonate rock
683 samples dated at the youngest from the Pleistocene and collected on the flat-top of the Munida
684 seamount that is currently submerged in 93 m water depth, are thought to be representative of
685 seismic unit UM-2 which would correspond to the last stage of the carbonate platform's growth.
686 Similarly to the Banc de la Torche and Antigonia, the flat-top of the eastern part of the Munida
687 seamount is currently located in the photic zone which suggests continuous carbonate
688 aggradation from the Miocene to the Quaternary. Such a continuous deposition was possibly
689 favoured by a slower subsidence at that location compared to other seamounts (Fig.13). The
690 Crypthelia seamount that is submerged at 194 m water depth is affected by three N160°E
691 normal faults scarps, leading to an overall eastward deepening of the seamount topography
692 along several stepped terraces at ca 200 m, 300 m and 350 m water depths (Fig.9A). The lack of
693 samples on these stepped terraces does not allow us to determine if the carbonate factory was
694 active during the Quaternary and when the isolated carbonate platform was drowned (Fig.13A).

695

6. CONCLUSIONS

The eastern margin of Grande Terre records the evolution of a shallow-water mixed carbonate-siliciclastic system, with the successive development an aggrading Mio-Pliocene carbonate bank and a backstepping Quaternary barrier reef.

- A Mio-Pliocene shallow-water carbonate platform, presently drowned at 300 to 600 m water depth, extends about 350 km from Ponerihouen to Antigonia seamount and can be up to 750 m thick along the Pines Ridge.

- In front of Grande Terre, the Mio-Pliocene carbonate sediments are mixed with quartz grains and ultrabasic pebbles, which document terrigenous inputs resulting from high relief of the island topography dismantling coeval with carbonate production as early as the Serravalian.

- The transition between the aggrading Mio-Pliocene carbonate bank and the backstepping Quaternary carbonate platforms along the eastern margin could be explained by the regional subsidence context driven by an extensional tectonic regime or by global climate change associated with Late Quaternary high-amplitude sea-level variations and/or changes of carbonate producers through time.

- The stratigraphic architectures of mixed carbonate-siliciclastic systems, represented by the Quaternary reef-lagoon complex along the upper slope, vary widely from north to south. In front of the Cap Bayes Pass, this contribution evidences for the first time in New Caledonia the presence of a lowstand terrigenous prism alternating with transgressive shallow-water carbonate sequence, typical to reciprocal sedimentation models. Nevertheless, this configuration is not observed southward, probably because other control parameters prevailed such as low terrigenous inputs, the particular morphology of the paleo-drainage network, which appears parallel to the coastline, or the high by-pass sediment transport toward the deep basin.

7. ACKNOWLEDGEMENTS

We thank Editor M. Rebesco, reviewer John J.G. Reijmer and an anonymous reviewer for their constructive comments on an early version of this paper. We are also grateful to John Butcher (IRD Nouméa) who provided access to samples.

REFERENCES

Adams, C.G., 1984. Neogene larger foraminifera, evolutionary and geological events in the context of datum planes, in: Ikebe, N., Tsuchi, R. (Eds.), Pacific Neogene Datum Planes. Tokyo, pp. 47–67.

Adams, E., Kenter, J.A.M., 2013. So different, yet so similar: comparing and contrasting siliciclastic and carbonate slopes, in: Verwer, K., Playton, T.E., Harris, P.M. (Eds.), Deposits, Architecture and Controls of Carbonate Margin, Slope and Basinal Settings, SEPM Special Publication. Tulsa, Oklahoma, pp. 14–25.

Aguirre, J., Riding, R., Braga, J.C., 2000. Diversity of coralline red algae: origination and extinction patterns from the Early Cretaceous to the Pleistocene. Paleobiology 26, 651–667. https://doi.org/10.1666/0094-8373(2000)026<0651:DOCRAO>2.0.CO;2

Andréfouët, S., Cabioch, G., Flamand, B., Pelletier, B., 2009. A reappraisal of the diversity of geomorphological and genetic processes of New Caledonian coral reefs: a synthesis from optical remote sensing, coring and acoustic multibeam observations. Coral Reefs 28, 691–707. https://doi.org/10.1007/s00338-009-0503-y

Anselmetti, F.S., Eberli, G.P., 2001. Sonic Velocity in Carbonates— A Combined Product of Depositional Lithology and Diagenetic Alterations, in: Ginsburg, R.N. (Ed.), Subsurface Geology of a Prograding Carbonate Platform Margin, Great Bahama Bank: Results of the Bahamas Drilling Project. SEPM Society for Sedimentary Geology, p. 0. https://doi.org/10.2110/pec.01.70.0193

Belde, J., Back, S., Bourget, J., Reuning, L., 2017. Oligocene and Miocene carbonate platform development in the Browse basin, Australian northwest shelf. Journal of Sedimentary Research 87, 795–816. https://doi.org/10.2110/jsr.2017.44

Bitoun, G., Recy, J., 1982. Origine et évolution du bassin des Loyauté et de ses bordures après la mise en place de la série ophiolitique de Nouvelle Calédonie, in: Contribution à l'étude Géodynamique Du Sud-Ouest Pacifique, Travaux et Documents ORSTOM. pp. 505–540.

Boudagher-Fadel, M.K., 2018a. Evolution and Geological Significance of Larger Benthic Foraminifera, Second edition. ed. UCL Press.

Boudagher-Fadel, M.K., 2018b. Revised diagnostic first and last occurrences of Mesozoic and Cenozoic planktonic foraminifera. UCL Office of the Vice-Provost Research, Professional Papers Series, UCL Press 1–5.

Boudagher-Fadel, M.K., 2015. Biostratigraphic and geological of planktonic foraminifera, Updated second edition. ed. UCP Press.

Boudagher-Fadel, M.K., Banner, F.T., 1999. Revision of the stratigraphic significance of the oligocene-miocene "Letter-Stages." Revue de Micropaléontologie 42, 93–97. https://doi.org/10.1016/S0035-1598(99)90095-8

Brachert, T.C., Forst, M.H., Pais, J.J., Legoinha, P., Reijmer, J.J.G., 2003. Lowstand carbonates, highstand sandstones? Sedimentary Geology 155, 1–12. https://doi.org/10.1016/S0037-0738(02)00329-9

Cabioch, G., Montaggioni, L., Frank, N., Seard, C., Sallé, E., Payri, C., Pelletier, B., Paterne, M., 2008a. Successive reef depositional events along the Marquesas foreslopes (French Polynesia) since 26 ka. Marine Geology 254, 18–34. https://doi.org/10.1016/j.margeo.2008.04.014

759 Cabioch, G., Montaggioni, L., Thouveny, N., Frank, N., Sato, T., Chazottes, V., Dalamasso, H., Payri, C., Pichon, M., Sémah,
760 A.-M., 2008b. The chronology and structure of the western New Caledonian barrier reef tracts. Palaeogeography,
761 Palaeoclimatology, Palaeoecology 268, 91–105. https://doi.org/10.1016/j.palaeo.2008.07.014

762 Cabioch, G., Pelletier, B., Boré, J.-M., Panché, J.-Y., Perrier, J., 2002a. Campagne Boisalis 1, Cartographie multifaisceaux et
763 dragages des pentes du récif barrière Est (Poindimié) et Sud-Est (Goro) de Nouvelle-Calédonie. Transport et
764 débarquement du matériel de forage sur l'îlot Bayes. (No. 44). Rapports de missions. Sciences de la Terre,
765 Géologie Géophysique, Centre IRD de Nouméa.

766 Cabioch, G., Pelletier, B., Perrier, J., Régnier, M., Varillon, D., 2002b. Campagne Boisalis 2, cartographie multifaisceaux et
767 dragages des pentes du récif barrière Sud-Est (Goro) et cartographie des passes de Mato et Boulari, Nouvelle-
768 Calédonie. (No. 45). Rapports de missions. Sciences de la Terre, Géologie Géophysique, Centre IRD de Nouméa.

769 Cabioch, G., Recy, J., Jouannic, C., Turpin, L., 1996. Controle climatique et tectonique de l'edification recifale en
770 Nouvelle-Caledonie au cours du Quaternaire terminal. Bulletin de la Société Géologique de France 167, 729–742.

771 Camoin, G.F., Seard, C., Deschamps, P., Webster, J.M., Abbey, E., Braga, J.C., Iryu, Y., Durand, N., Bard, E., Hamelin, B.,
772 Yokoyama, Y., Thomas, A.L., Henderson, G.M., Dussouillez, P., 2012. Reef response to sea-level and environmental
773 changes during the last deglaciation: Integrated Ocean Drilling Program Expedition 310, Tahiti Sea Level.
774 Geology 40, 643–646. https://doi.org/10.1130/G32057.1

775 Chaisson, W.P., Ravelo, A.C., 1997. Changes in upper water-column structure at Site 925, late Miocene–
776 Pleistocene:planktonic foraminifer assemblage and isotopic evidence, in: Shackleton, N.J., Curry, W.B., Richter, C.,
777 Bralower, T.J. (Eds.), Proceedings of the Ocean Drilling Program, Scientific Results, Ocean Drilling Program.
778 College Station, TX, pp. 255–268.

779 Chardon, D., Austin, J.A., Cabioch, G., Pelletier, B., Saustrup, S., 2007. NEOMARGES, Imagerie sismique du lagon et des
780 pentes des marges de la ride de Nouvelle-Calédonie à travers le récif barrière de la Grande Terre, 12-21
781 décembre 2006 (Rapport de missions, Sciences de la Terre, Géologie-Géophysique No. 72). IRD.
782 https://doi.org/10.17600/6100140

783 Chardon, D., Austin, J.A., Cabioch, G., Pelletier, B., Saustrup, S., Sage, F., 2008. Neogene history of the northeastern New
784 Caledonia continental margin from multichannel reflection seismic profiles. Comptes Rendus Geoscience 340,
785 68–73. https://doi.org/10.1016/j.crte.2007.09.017

786 Chardon, D., Chevillotte, V., 2006. Morphotectonic evolution of the New Caledonia ridge (Pacific Southwest) from post-
787 obduction tectonosedimentary record. Tectonophysics 420, 473–491.
788 https://doi.org/10.1016/j.tecto.2006.04.004

789 Chevillon, C., 1997. Sédimentologie descriptive et cartographie des fonds meubles du lagon de la côte Est de Nouvelle-
790 Calédonie, in: Les Fonds Meubles Des Lagons de Nouvelle-Calédonie (Sédimentologie, Benthos), Etudes et
791 Thèses, ORSTOM. pp. 7–30.

792 Chiarella, D., Longhitano, S.G., Tropeano, M., 2017. Types of mixing and heterogeneities in siliciclastic-carbonate
793 sediments. Marine and Petroleum Geology 88, 617–627. https://doi.org/10.1016/j.marpetgeo.2017.09.010

794 Cluzel, D., Aitchison, J.C., Picard, C., 2001. Tectonic accretion and underplating of mafic terranes in the Late Eocene
795 intraoceanic fore-arc of New Caledonia (Southwest Pacific): geodynamic implications. Tectonophysics 340, 23–
796 59. https://doi.org/10.1016/S0040-1951(01)00148-2

797 Cluzel, D., Bosch, D., Paquette, J.-L., Lemennicier, Y., Montjoie, P., Ménot, R.-P., 2005. Late Oligocene post-obduction
798 granitoids of New Caledonia: A case for reactivated subduction and slab break-off. Island Arc 14, 254–271.
799 https://doi.org/10.1111/j.1440-1738.2005.00470.x

800 Cohen, K.M., Harper, D.A.T., Gibbard, P.L., 2017. ICS International Chronostratigraphic Chart 2017/02.

801 Collot, J., Patriat, M., Etienne, S., Rouillard, P., Soetaert, F., Juan, C., Marcaillou, B., Palazzin, G., Clerc, C., Maurizot, P.,
802 Pattier, F., Tournadour, E., Sevin, B., Privat, A., 2017. Deepwater Fold-and-Thrust Belt Along New Caledonia's
803 Western Margin: Relation to Post-obduction Vertical Motions. Tectonics 36, 2108–2122.
804 https://doi.org/10.1002/2017TC004542

Collot, J.Y., Malahoff, A., Recy, J., Latham, G., Missegue, F., 1987. Overthrust emplacement of New Caledonia Ophiolite: Geophysical evidence. Tectonics 6, 215–232. https://doi.org/10.1029/TC006i003p00215

Cotillon, P., Coustillas, F., Gaillard, C., Laurin, B., Liu, D.-J., Pannetier, W., Rigolot, P., Pascal, A., Pascal, F., 1990. Grands traits de la sedimentation actuelle et recente sur les pentes et dans les bassins au large de la Nouvelle Caledonie (SW Pacifique): Resultats geologiques de la campagne Biocal Cotillon P, Coustillas F, Gaillard C, Laurin B, Liu D-J, Pannetier W, Rigolot P, Pascal A, Pascal F. Oceanologica Acta, Special issue (0399-1784) Actes du Colloque Tour du monde Jean Charcot, Paris (France), 2-3 Mar 1989.

Cotillon, P., Liu, J.D., Gaillard, C., Evin, J., 1989. Evolution du taux de sedimentation au cours des derniers 30 000 ans aux abords de la Nouvelle-Caledonie (SW Pacifique); resultats de datations au radiocarbone et par la courbe de l'oxygene 18. Bulletin de la Société Géologique de France V, 881–884. https://doi.org/10.2113/gssgfbull.V.4.881

Coudray, J., 1976. Recherches sur le Neogene et le Quaternaire marins de la Nouvelle-Calédonie; contribution de l'étude sédimentologique a la connaissance de l'histoire géologique post-Eocene, in: Expédition Française Sur Les Récifs Nouvelle-Calédonie, Fond. Singer-Polignac. Paris, pp. 1–276.

Coudray, J., 1975. Recherches sur le Néogène et le Quaternaire marin de la Nouvelle-Calédonie. Contribution de l'étude sédimentologique à la connaissance de l'histoire géologique post-éocène (Thèse de Doctorat). Université des Sciences et Techniques du Languedoc.

Daniel, J., Dugas, F., Dupont, J., Jouannic, C., Launay, J., Monzier, M., Recy, J., 1976. La zone charnière Nouvelle-Calédonie - ride de Norfolk (S.W. Pacifique) : résultats de dragages et interprétation. Cahiers ORSTOM série Géologie 8, 95–105.

Droxler, A.W., Jorry, S.J., 2013. Deglacial Origin of Barrier Reefs Along Low-Latitude Mixed Siliciclastic and Carbonate Continental Shelf Edges. Annu. Rev. Mar. Sci. 5, 165–190. https://doi.org/10.1146/annurev-marine-121211-172234

Dubois, J., Launay, J., Recy, J., 1975. Some new evidence on lithospheric bulges close to island arcs. Tectonophysics 26, 189–196. https://doi.org/10.1016/0040-1951(75)90089-X

Dubois, J., Launay, J., Recy, J., 1974. Uplift movements in New Caledonia-Loyalty Islands area and their plate tectonics interpretation. Tectonophysics 24, 133–150. https://doi.org/10.1016/0040-1951(74)90134-6

Dunbar, G.B., Dickens, G.R., 2003. Massive siliciclastic discharge to slopes of the Great Barrier Reef Platform during sea-level transgression: constraints from sediment cores between 15°S and 16°S latitude and possible explanations. Sediment. Geol. 162, 141–158. https://doi.org/10.1016/S0037-0738(03)00216-1

Ehrenberg, S.N., McArthur, J.M., Thirlwall, M.F., 2006. Growth, Demise, and Dolomitization of Miocene Carbonate Platforms on the Marion Plateau, Offshore NE Australia. Journal of Sedimentary Research 76, 91–116. https://doi.org/10.2110/jsr.2006.06

Esker, D.E., Eberli, G.P., McNeill, D.F., 1998. The Structural and Sedimentological Controls on the Reoccupation of Quaternary Incised Valleys, Belize Southern Lagoon. AAPG Bull. 82, 2075–2109. https://doi.org/10.1306/00AA7BE4-1730-11D7-8645000102C1865D

Ferro, C.E., Droxler, A.W., Anderson, J.B., Mucciarone, D., 1999. Late Quaternary shift of mixed siliciclastic-carbonate environments induced by glacial eustatic sea-level fluctuations in Belize. In: Advances in carbonate sequence stratigraphy: Application to reservoirs, outcrops and models (Eds P.M. Harris, A.H. Saller and T. Simo), SEPM Special Publication v. 63, pp. 385-411. SEPM (Society for Sedimentary Geology), Tulsa.

Flamand, B., 2006. Les pentes externes du récif barrière de la Grande Terre de Nouvelle-Calédonie : morphologie, lithologie, contrôle de la tectonique et de l'eustatisme. Université de Bretagne occidentale, Brest, France.

Frank, N., Turpin, L., Cabioch, G., Blamart, D., Tressens-Fedou, M., Colin, C., Jean-Baptiste, P., 2006. Open system U-series ages of corals from a subsiding reef in New Caledonia: Implications for sea level changes, and subsidence rate. Earth and Planetary Science Letters 249, 274–289. https://doi.org/10.1016/j.epsl.2006.07.029

Fürstenau, J., Lindhorst, S., Betzler, C., Hübscher, C., 2010. Submerged reef terraces of the Maldives (Indian Ocean). Geo-Mar Lett 30, 511–515. https://doi.org/10.1007/s00367-009-0174-2

Gaina, C., Müller, D.R., Royer, J.-Y., Stock, J., Hardebeck, J., Symonds, P., 1998. The tectonic history of the Tasman Sea: A puzzle with 13 pieces. Journal of Geophysical Research: Solid Earth 103, 12413–12433. https://doi.org/10.1029/98JB00386

Geldart, L.P., Sheriff, R.E., 2004. Problems in Exploration Seismology and their Solutions. Society of Exploration Geophysicists. https://doi.org/10.1190/1.9781560801733

Gischler, E., Ginsburg, R.N., Herrle, J.O., Prasad, S., 2010. Mixed carbonates and siliciclastics in the Quaternary of southern Belize: Pleistocene turning points in reef development controlled by sea-level change. Sedimentology 57, 1049–1068. https://doi.org/10.1111/j.1365-3091.2009.01133.x

Gradstein, F.M., Ogg, J.G., Schmitz, M.D., Ogg, G.M. (Eds.), The Geologic Time Scale. Elsevier, Boston, pp. ix–xi. https://doi.org/10.1016/B978-0-444-59425-9.10003-4

Hallock, P., Schlager, W., 1986. Nutrient Excess and the Demise of Coral Reefs and Carbonate Platforms. PALAIOS 1, 389. https://doi.org/10.2307/3514476

Harper, B.B., Puga-Bernabéu, Á., Droxler, A.W., Webster, J.M., Gischler, E., Tiwari, M., Lado-Insua, T., Thomas, A.L., Morgan, S., Jovane, L., Röhl, U., 2015. Mixed Carbonate–Siliciclastic Sedimentation Along the Great Barrier Reef Upper Slope: A Challenge To the Reciprocal Sedimentation Model. Journal of Sedimentary Research 85, 1019–1036. https://doi.org/10.2110/jsr.2015.58.1

Hayes, D.E., Ringis, J., 1973. Seafloor Spreading in the Tasman Sea. Nature 243, 454–458. https://doi.org/10.1038/243454a0

Hohenegger, J., 2005. Estimation of environmental paleogradient values based on presence/absence data: a case study using benthic foraminifera for paleodepth estimation. Palaeogeogr. Palaeoclimatol. Palaeoecol. 217, 115–130. https://doi.org/10.1016/j.palaeo.2004.11.020

Hohenegger, J., 1995. Depth estimation by proportions of living larger foraminifera. Mar. Micropal. 26, 31–47. https://doi.org/10.1016/0377-8398(95)00044-5

Hottinger, L., 1983. Processes determining the distribution of larger foraminifera in space and time. Utrecht Micropal. Bull. 30, 239–253.

Jorry, S.J., Camoin, G.F., Jouet, G., Roy, P.L., Vella, C., Courgeon, S., Prat, S., Fontanier, C., Paumard, V., Boulle, J., Caline, B., Borgomano, J., 2016. Modern sediments and Pleistocene reefs from isolated carbonate platforms (Iles Eparses, SW Indian Ocean): A preliminary study. Acta Oecologica 72, 129–143. https://doi.org/10.1016/j.actao.2015.10.014

Juffroy, F., 2009. Atlas bathymétrique de la Nouvelle-Calédonie. Rapport du Service de la Géomatique et de la Télédétection du Gouvernement de la Nouvelle-Calédonie.

Kerans, C., Tinker, S.W., 1999. Extrinsic Stratigraphic Controls on Development of the Capitan Reef Complex, in: Saller, A.H., Harris, P.M. (Mitch), Kirkland, B.L., Mazzullo, S.J. (Eds.), Geologic Framework of the Capitan Reef. SEPM Society for Sedimentary Geology, p. 0.

Khanna, P., Droxler, A.W., Nittrouer, J.A., Tunnell Jr, J.W., Shirley, T.C., 2017. Coralgal reef morphology records punctuated sea-level rise during the last deglaciation. Nature Communications 8, 1046. https://doi.org/10.1038/s41467-017-00966-x

Lafoy, Y., Missègue, F., Cluzel, D., Voisset, M., Saget, P., Lenoble, J.-P., Rigaut, F., Lanckneus, J., Lehodey, P., Bouniot, E., Cornec, J., De Souza, K., Gallois, F., Garioud, N., Grenard, P., N'Diaye, M., Perchoc, Y., Perrier, J., 1994. Campagne ZoNéCo 2 (2 au 22 août 1994), RV L'Atalante.

Lafoy, Y., Van de Beuque, S., Missègue, F., Nercessian, A., Bernardel, G., 1998. Campagne de sismique multitraces entre la marge Est Australienne et le Sud de l'Arc des Nouvelles-Hébrides Rapport de la campagne RIG SEISMIC 206 (21 avril - 24 mai 1998), Programme FAUST (French Australian Seismic Transect). Programme ZoNéCo.

Lagabrielle, Y., Chauvet, A., 2008. The role of extensional tectonics in shaping Cenozoic New-Caledonia. Bulletin de la Société Géologique de France 179, 315–329. https://doi.org/10.2113/gssgfbull.179.3.315

Lagabrielle, Y., Maurizot, P., Lafoy, Y., Cabioch, G., Pelletier, B., Régnier, M., Wabete, I., Calmant, S., 2005. Post-Eocene extensional tectonics in Southern New Caledonia (SW Pacific): Insights from onshore fault analysis and offshore seismic data. Tectonophysics 403, 1–28. https://doi.org/10.1016/j.tecto.2005.02.014

Launay, J., 1985. Paléoniveaux marins et néotectonique à l'île des Pins (Nouvelle -Calédonie). Géologie de la France 1, 77–81.

Le Roy, P., Cabioch, G., Monod, B., Lagabrielle, Y., Pelletier, B., Flamand, B., 2008. Late Quaternary history of the Nouméa lagoon (New Caledonia, South West Pacific) as depicted by seismic stratigraphy and multibeam bathymetry: A modern model of tropical rimmed shelf. Palaeogeography, Palaeoclimatology, Palaeoecology 270, 29–45. https://doi.org/10.1016/j.palaeo.2008.08.012

Le Roy, P., Jorry, S., Jouet, G., Ehrhold, A., Michel, G., Gautier, V., Guérin, C., 2019. Late Pleistocene evolution of the mixed siliciclastic and carbonate southwestern New Caledonia continental shelf/lagoon. Palaeogeography, Palaeoclimatology, Palaeoecology 514, 502–521. https://doi.org/10.1016/j.palaeo.2018.10.014

Mallarino, G., Francis, J.M., Jorry, S.J., Daniell, J.J., Droxler, A.W., Dickens, G.R., Beaufort, L., Bentley, S.J., Opdyke, B.N., Peterson, L.C., 2021. Timescale dependent sedimentary record during the past 130 kyr from a tropical mixed siliciclastic–carbonate shelf edge and slope: Ashmore Trough (southern Gulf of Papua). Sedimentology sed.12867. https://doi.org/10.1111/sed.12867

Maurizot, P., Cabioch, G., Fournier, F., Leonide, P., Sebih, S., Rouillard, P., Montaggioni, L., Collot, J., Martin-Garin, B., Chaproniere, G., Braga, J.C., Sevin, B., 2016. Post-obduction carbonate system development in New Caledonia (Népoui, Lower Miocene). Sedimentary Geology 331, 42–62. https://doi.org/10.1016/j.sedgeo.2015.11.003

Maurizot, P., Collot, J., Cluzel, D., Patriat, M., 2020. Chapter 6 The Loyalty Islands and Ridge, New Caledonia. Geological Society, London, Memoirs 51, 131. https://doi.org/10.1144/M51-2017-24

Maurizot, P., Vendé-Leclerc, M., 2009. New Caledonia geological map, scale 1/500000. Direction de l'Industrie, des Mines et de l'Energie-Service de la Géologie de Nouvelle-Calédonie, Bureau de Recherches Géologiques et Minières.

McCaffrey, J.C., Wallace, M.W., Gallagher, S.J., 2020. A Cenozoic Great Barrier Reef on Australia's North West shelf. Global and Planetary Change 184, 103048. https://doi.org/10.1016/j.gloplacha.2019.103048

McKee, E.D., Oriel, S.S., Ketner, K.B., MacLachlan, M.E., Goldsmith, J.W., MacLachlan, J.C., Mudge, M.R., 1959. Paleotectonic maps of the Triassic System. Miscellaneous Geologic Investigations Map.

McKenzie, J.A., Spezzaferri, S., Isern, A., 1999. The Miocene-Pliocene boundary in the Mediterranean Sea and Bahamas; implications for a global flooding event in the earliest Pliocene. Memorie della Società Geologica Italiana 54, 93–108.

McNeill, D.F., Pisera, A., 2010. Neogene Lithofacies Evolution on a Small Carbonate Platform in the Loyalty Basin, Mare, New Caledonia, in: Morgan, W.A., George, A.D., Harris, P.M. (Mitch), Kupecz, J.A., Sarg, J.F. (Rick) (Eds.), Cenozoic Carbonate Systems of Australasia. SEPM Society for Sedimentary Geology, p. 0.

Missègue, F., Saget, P., Desrus, M., Le Suavé, R., Lafoy, Y., 1996. Mission ZoNéCo 3 (30 Aout au 20 Septembre 1996), RV L'Atalante. https://doi.org/10.17600/96010070

Mitchell, J.K., Holdgate, G.R., Wallace, M.W., Gallagher, S.J., 2007. Marine geology of the Quaternary Bass Canyon system, southeast Australia: A cool-water carbonate system. Mar. Geol. 237, 71–96. https://doi.org/10.1016/j.margeo.2006.10.037

Mitchum, R.M., Vail, P.R., Sangree, J.B., 1977. Seismic stratigraphy and global changs of sea-level, part 6: stratigraphic interpretation of seismic reflectionpatterns in depositional sequences, part 6, in: Payton, C.E. (Ed.), Seismic Stratigraphy: Applications to Hydrocarbon Exploration, AAPG Memoir. pp. 117–133.

Montaggioni, L.F., Cabioch, G., Thouveny, N., Frank, N., Sato, T., Sémah, A.-M., 2011. Revisiting the Quaternary development history of the western New Caledonian shelf system: From ramp to barrier reef. Marine Geology 280, 57–75. https://doi.org/10.1016/j.margeo.2010.12.001

Moretti, I., Turcotte, D.L., 1985. A model for erosion, sedimentation, and flexure with application to New Caledonia. Journal of Geodynamics 3, 155–168. https://doi.org/10.1016/0264-3707(85)90026-2

Mortimer, N., Campbell, H., Tulloch, A.J., King, P.R., Stagpoole, V.M., Wood, R.A., Rattenbury, M.S., Sutherland, R., Adams, C.J., Collot, J., Seton, M., 2017. Zealandia: Earth's Hidden Continent. The Geological Society of America 27, 27–35.

Nebelsick, J.H., Stingl, V., Rasser, M., 2001. Autochthonous facies and allochthonous debris flows compared: Early oligocene carbonate facies patterns of the Lower Inn Valley (Tyrol, Austria). Facies 44, 31. https://doi.org/10.1007/BF02668165

O'Connell, B., Dorsey, R.J., Hasiotis, S.T., Hood, A.V.S., 2021. Mixed carbonate–siliciclastic tidal sedimentation in the Miocene to Pliocene Bouse Formation, palaeo-Gulf of California. Sedimentology 68, 1028–1068. https://doi.org/10.1111/sed.12817

Paquette, J.-L., Cluzel, D., 2007. U–Pb zircon dating of post-obduction volcanic-arc granitoids and a granulite-facies xenolith from New Caledonia. Inference on Southwest Pacific geodynamic models. International Journal of Earth Sciences 96, 613–622. https://doi.org/10.1007/s00531-006-0127-1

Paris, J.P., 1981. Géologie de la Nouvelle-Calédonie, Un essai de synthèse, Mémoire du BRGM. Orléans, France.

Patriat, M., Collot, J., Etienne, S., Poli, S., Clerc, C., Mortimer, N., Pattier, F., Juan, C., Roest, W.R., VESPA scientific voyage team, 2018. New Caledonia Obducted Peridotite Nappe: Offshore Extent and Implications for Obduction and Postobduction Processes. Tectonics 37, 1077–1096. https://doi.org/10.1002/2017TC004722

Pautot, G., Lafoy, Y., Dupont, J., Le Suavé, R., 1993. Campagne ZoNéCo 1 (25 juin au 16 juillet 1993), RV L'Atalante. https://doi.org/10.17600/93000130

Pelletier, B., Butscher, J., Panché, J.-Y., Perrier, J., Maloune, A., 2002. Cartographie au sondeur multifaisceaux des pentes externes du récif barrière de la Province Nord de la Nouvelle-Calédonie. Campagne Province Nord 1, côte Est de la passe de Thio à la passe de Balade (24 juillet au 1er août 2002). (No. 48). Rapports de missions, Sciences de la Terre, Géologie-Géophysique, Centre IRD Nouméa.

Pelletier, B., Cabioch, G., Chardon, D., Yamano, H., 2006. Lithologie des pentes externes du récif barrière de Nouvelle-Calédonie. Campagne de dragages « 2005-NC-DR » du N.O. Alis (30 mai – 7 juin 2005). (No. 68). Rapports de missions, Sciences de la Terre, Géologie Géophysique, Centre IRD de Nouméa.

Pelletier, B., Juffroy, F., Flamand, B., Perrier, J., 2012. La bathymétrie des marges de la Grande Terre et des îles Loyauté. Planche 5., in: Bonvallot, J., Gay, J.C., Habert, E. (Eds.), Atlas de La Nouvelle Calédonie. Nouméa : IRD ; Congrès de la Nouvelle-Calédonie, Marseille (FRA), pp. 33–36.

Pelletier, B., Perrier, J., Juffroy, F., Flamand, B., Panché, J.-Y., Gallois, F., 2004. Cartographie systématique par sondeur multifaisceaux des pentes externes du récif barrière de la Grande Terre et des Iles Loyauté, Nouvelle-Calédonie. Assises de la Recherche Française dans le Pacifique, 24-27 aout 2004, Nouméa, Nouvelle-Calédonie. Résumés des communications scientifiques, p.271-272. Poster. Presented at the Assises de la Recherche Française dans le Pacifique, 24-27 aout 2004, Nouméa, Nouvelle-Calédonie.

Perrier, J., Flamand, B., Juffroy, F., Panché, J.-Y., Le Houarno, H., 2004a. Cartographie au sondeur multifaisceaux de la zone côtière de la Province Sud. Campagne Province Sud 1, N.O. Alis (2-5 février et 11-20 février 2004). (No. 62). Rapports de missions, Sciences de la Terre, Géologie-Géophysique, Centre IRD Nouméa.

Perrier, J., Flamand, B., Robineau, B., Panché, J.-Y., Le Houarno, H., 2004b. Cartographie au sondeur multifaisceaux de la zone côtière de la Province Sud, Campagne Province Sud 2. N.O. Alis du 23 septembre au 2 octobre 2004. Côte Ouest: de la passe de Boulari à la passe Koko; Sud: Corne Sud. (No. 63), Rapports de missions, Sciences de la Terre, Géologie-Géophysique, Centre IRD de Nouméa.

Perrier, J., Panché, J.-Y., Juffroy, F., Barazer, J.-F., 2005. Cartographie au sondeur multifaisceaux de la zone côtière de la Province Sud. Campagne Province Sud 4, NO Alis. 21 au 24 septembre 2005. Hauts fonds à l'extrémité sud de la Grande Terre : Banc 93, Banc Antigonia, Mont 1 (No. 65). Rapports de missions Sciences de la Terre. Géologie Géophysique, Centre IRD de Nouméa.

Perrier, J., Pelletier, B., Panché, J.-Y., Barazer, J.-F., Juffroy, F., 2004c. Cartographie au sondeur multifaisceaux de la zone côtière de la Province Sud. Campagne Province Sud 3, N.O. Alis du 26 novembre au 30 novembre 2004. Côte Sud Est : de la passe de la Sarcelle à la terminaison sud de l'île des Pins (banc de la Torche). (No. 64). Rapports de missions, Sciences de la Terre, Géologie-Géophysique, Centre IRD de Nouméa.

990 Puillandre, N., Samadi, S., 2016. Kanacono cruise, RV Alis,. https://doi.org/10.17600/16003900

991 Purdy, E.G., Gischler, E., 2005. The transient nature of the empty bucket model of reef sedimentation. Sedimentary
992 Geology 175, 35–47. https://doi.org/10.1016/j.sedgeo.2005.01.007

993 Rigolot, P., 1989. Origine et évolution du "système" ride de Nouvelle-Calédonie/Norfolk (Sud -Ouest Pacifique) :
994 synthèse des données de géologie et de géophysique marine. Etude des marges et bassins associés. UBO, Brest.

995 Rovere, A., Khanna, P., Bianchi, C.N., Droxler, A.W., Morri, C., Naar, D.F., 2018. Submerged reef terraces in the Maldivian
996 Archipelago (Indian Ocean). Geomorphology 317, 218–232. https://doi.org/10.1016/j.geomorph.2018.05.026

997 Schlager, W., 1989. Drowning Unconformities on Carbonate Platforms, in: Controls on Carbonate Platforms and Basin
998 Development, SEPM SPECIAL PUBLICATION.

999 Sevin, B., Maurizot, P., Cluzel, D., Tournadour, E., Etienne, S., Folcher, N., Jeanpert, J., Collot, J., Iseppi, M., Meffre, S.,
1000 Patriat, M., 2020. Chapter 7 Post-obduction evolution of New Caledonia. Geological Society, London, Memoirs
1001 51, 147. https://doi.org/10.1144/M51-2018-74

1002 Smith, W.H.F., Sandwell, D.T., 1997. Global Sea Floor Topography from Satellite Altimetry and Ship Depth Soundings.
1003 Science 277, 1956. https://doi.org/10.1126/science.277.5334.1956

1004 Sutherland, R., Viskovic, G.P.D., Bache, F., Stagpoole, V.M., Collot, J., Rouillard, P., Hashimoto, T., Hackney, R., Rollet, N.,
1005 Patriat, M., Roest, W.R., 2012. Compilation of seismic reflection data from the Tasman Frontier region, southwest
1006 Pacific (GNS Sciense Report No. 2012/01).

1007 Tcherepanov, E.N., Droxler, A.W., Lapointe, P., Dickens, G.R., Bentley, S.J., Beaufort, L., Peterson, L.C., Daniell, J., Opdyke,
1008 B.N., 2008a. Neogene evolution of the mixed carbonate-siliciclastic system in the Gulf of Papua, Papua New
1009 Guinea. J. Geophys. Res. 113, F01S21. https://doi.org/10.1029/2006JF000684

1010 Tcherepanov, E.N., Droxler, A.W., Lapointe, P., Mohn, K., 2008b. Carbonate seismic stratigraphy of the Gulf of Papua
1011 mixed depositional system: Neogene stratigraphic signature and eustatic control. Basin Res. 20, 185–209.
1012 https://doi.org/10.1111/j.1365-2117.2008.00364.x

1013 Tcherepanov, E.N., Droxler, A.W., Lapointe, P., Mohn, K., Larsen, O.A., 2010. Siliciclastic influx and burial of the Cenozoic
1014 carbonate system in the Gulf of Papua. Marine and Petroleum Geology 27, 533–554.
1015 https://doi.org/10.1016/j.marpetgeo.2009.09.002

1016 Teillet, T., Fournier, F., Borgomano, J., Hong, F., 2020a. Origin of seismic reflections in a carbonate gas field, Lower
1017 Miocene, offshore Myanmar. Marine and Petroleum Geology 113, 104110.
1018 https://doi.org/10.1016/j.marpetgeo.2019.104110

1019 Teillet, T., Fournier, F., Montaggioni, L.F., BouDagher-Fadel, M., Borgomano, J., Braga, J.C., Villeneuve, Q., Hong, F.,
1020 2020b. Development patterns of an isolated oligo-mesophotic carbonate buildup, early Miocene, Yadana field,
1021 offshore Myanmar. Marine and Petroleum Geology 111, 440–460.
1022 https://doi.org/10.1016/j.marpetgeo.2019.08.039

1023 Terry, J.P., Wotling, G., 2011. Rain-shadow hydrology: Influences on river flows and flood magnitudes across the
1024 central massif divide of La Grande Terre Island, New Caledonia. Journal of Hydrology 404, 77–86.
1025 https://doi.org/10.1016/j.jhydrol.2011.04.022

1026 Toomey, M.R., Woodruff, J.D., Donnelly, J.P., Ashton, A.D., Perron, J.T., 2016. Seismic evidence of glacial-age river
1027 incision into the Tahaa barrier reef, French Polynesia. Marine Geology 380, 284–289.
1028 https://doi.org/10.1016/j.margeo.2016.04.008

1029 Tournadour, E., Fournier, F., Etienne, S., Collot, J., Maurizot, P., Patriat, M., Sevin, B., Morgans, H.E.G., Martin-Garin, B.,
1030 Braga, J.C., 2020. Seagrass-related carbonate ramp development at the front of a fan delta (Burdigalian, New
1031 Caledonia): Insights into mixed carbonate-siliciclastic environments. Marine and Petroleum Geology 121,
1032 104581. https://doi.org/10.1016/j.marpetgeo.2020.104581

1033 Wallace, M.W., Holdgat, G.R., Daniels, J., Gallagher, S.J., Smith, A., 2002. Sonic velocity, submarine canyons, and burial
1034 diagenesis in Oligocene-Holocene cool-water carbonates, Gippsland Basin, southeast Australia. AAPG Bull. 86,
1035 1593–1607. https://doi.org/10.1306/61EEDD14-173E-11D7-8645000102C1865D

Webster, J.M., Braga, J.C., Humblet, M., Potts, D.C., Iryu, Y., Yokoyama, Y., Fujita, K., Bourillot, R., Esat, T.M., Fallon, S., Thompson, W.G., Thomas, A.L., Kan, H., McGregor, H.V., Hinestrosa, G., Obrochta, S.P., Lougheed, B.C., 2018. Response of the Great Barrier Reef to sea-level and environmental changes over the past 30,000 years. Nature Geoscience 11, 426–432. https://doi.org/10.1038/s41561-018-0127-3

Weij, R., Reijmer, J.J.G., Eberli, G.P., Swart, P.K., 2019. The limited link between accommodation space, sediment thickness, and inner platform facies distribution (Holocene–Pleistocene, Bahamas). The Depositional Record 5, 400–420. https://doi.org/10.1002/dep2.50

Wilson, J.L., 1967. Cyclic and Reciprocal Sedimentation in Virgilian Strata of Southern New Mexico. GSA Bulletin 78, 805–818. https://doi.org/10.1130/0016-7606(1967)78[805:CARSIV]2.0.CO;2

Wilson, P.A., Roberts, H.H., 1995. Density cascading; off-shelf sediment transport, evidence and implications, Bahama Banks. Journal of Sedimentary Research 65, 45–56. https://doi.org/10.1306/D426801D-2B26-11D7-8648000102C1865D

Wilson, P.A., Roberts, H.H., 1992. Carbonate-periplatform sedimentation by density flows: A mechanism for rapid off-bank and vertical transport of shallow-water fines. Geology 20, 713–716. https://doi.org/10.1130/0091-7613(1992)020<0713:CPSBDF>2.3.CO;2

Yamano, H., Cabioch, G., Pelletier, B., Chevillon, C., Tachikawa, H., Lefêvre, J., Marchesiello, P., 2015. Modern carbonate sedimentary facies on the outer shelf and slope around New Caledonia. Island Arc 24, 4–15. https://doi.org/10.1111/iar.12085

Yordanova, E.K., Hohenegger, J., 2007. Studies on settling, traction and entrainment of larger benthic foraminiferal tests: implications for accumulation in shallow marine sediments. Sedimentology 54, 1273–1306. https://doi.org/10.1111/j.1365-3091.2007.00881.x

Yordanova, E.K., Hohenegger, J., 2002. Taphonomy of larger foraminifera: Relationships between living individuals and empty tests on flat reef slopes (Sesoko Island, Japan). Facies 46, 169–203. https://doi.org/10.1007/BF02668080

Zeller, M., Verwer, K., Eberli, G.P., Massaferro, J.L., Schwarz, E., Spalletti, L., 2015. Depositional controls on mixed carbonate–siliciclastic cycles and sequences on gently inclined shelf profiles. Sedimentology 62, 2009–2037. https://doi.org/10.1111/sed.12215

Zinke, J., Reijmer, J.J.G., Thomassin, B.A., 2001. Seismic architecture and sediment distribution within the Holocene barrier reef–lagoon complex of Mayotte (Comoro archipelago, SW Indian Ocean). Palaeogeography, Palaeoclimatology, Palaeoecology 175, 343–368. https://doi.org/10.1016/S0031-0182(01)00379-0

FIGURE AND TABLE CAPTIONS

Figure 1: A. Regional location map of the study area. **B.** Simplified geological map of Grande Terre, New Caledonia (modified after Maurizot and Vendé-Leclerc, 2009) and shaded bathymetric map of surrounding offshore areas with the southern extensions of the Peridotite Nappe and metamorphic belt (Pines and Félicité ridges, respectively; after Patriat et al., 2018). Drill sites of the Quaternary barrier reef (Coudray, 1975; Cabioch et al., 2008; Montaggioni et al., 2011) and outcrops of the Lower Miocene mixed carbonate siliciclastic systems of Népoui are also indicated (Maurizot et al., 2016 ; Tournadour et al., 2020). **C.** Simplified SW to NE oriented geological cross-section of Grande Terre (modified after Lagabrielle et al., 2005 and Collot et al., 1987). N: Nouméa ; Pn: Ponérihouen ; Th: Thio ; Yt: Yaté ; IP: Isle of Pines ; T : Banc de la Torche ; S : Stylaster seamount ; B : Brachiopod seamount ; A : Antigonia seamount ; C : Crypthelia seamount ; M : Munida seamount.

Figure 2: Bathymetric map of the eastern margin of Grande Terre, from Poindimié to the Pines Ridge with location of the dataset used in this study including seismic profiles AUS-104 (Bitoun & Recy, 1982), 206-04 (dashed black lines), NEOMARGES (Chardon, 2006; Chardon et al. 2008, black lines), and dredged carbonate samples (yellow circles). T : Banc de la Torche ; S : Stylaster seamount ; B : Brachiopod seamount ; A : Antigonia seamount ; C : Crypthelia seamount ; M : Munida seamount.

Figure 3: A. Bathymetric map of the eastern lagoon of Grande Terre from Ponérihouen to Yaté. On the outer slope, note the terrace mapped in orange between 300 to 600 m water depths. **B.** Bathymetrical profile across the lagoon from the coast of Houailou to the outer barrier reef (see location on Figure A) showing three main morphobathymetric zones: 1) a shallow-water coastal zone dominated by fine-grained terrigenous sediments; 2) a deeper median lagoon with aligned islands and a coast-parallel channel network in front of Cote Oubliée; 3) a barrier reef domain cross-cut by passes, dominated by coarse-grained carbonate sedimentation. D: Deltas; D*:

Restricted deltas; SI: Sandy Islets; PR: Patch Reefs. Red lines are positions of seismic profiles. Yellow circles are positions of dredged carbonate samples.

Figure 4: Typical bathymetric profiles of the outer slopes of Grande Terre (location on Fig.2) highlighting the very steep character of the western margin (dashed green lines; W-01 and W-02) contrasting with the more gently inclined eastern margin (solid blue lines; E-01 and E-02). The latter illustrate the main morpho-bathymetric domains of the eastern margin slope, which can be divided into a low gradient (2-3°) upper slope mostly preserved from erosion, a middle slope affected by numerous submarine canyons and a lower slope to to-of-slope region. The hatched area shows the elevation difference between the southern and central parts of the eastern margin (E-01 and E-02, respectively), highlighting that the slope is better preserved from retrogressive erosion by slope canyons processes towards the south.

Figure 5: A. 3D bathymetrical map of the outer slope in front of Cap Bayes Pass with location of dip-oriented seismic profile NM-1. **B.** Seismic profile NM-1 profile with location of quaternary terraces (blue arrow, see details in Flamand, 2006), clinoform slope break of U2 prism (green arrow) and the bathymetrical scarp associated with the top of U1 seismic unit (red arrow). **C.** Interpretation of seismic profile NM-1 highlighting five sub-units inside U2, interpreted as parasequences (numbered from 1 to 5). Each parasequence is typified by an alternation of lowstand forced regressive wedges (in beige) and aggrading to retrograding shallow-water carbonate transgressive sequences (in pink), consistent with the pattern of reciprocal sedimentation model.

Figure 6: A. 3D bathymetrical map of the outer slope in front of Canala with location of seismic profiles NM-4 and NM-9 and dredged carbonate rocks (see Table 3). **B.** Uninterpreted seismic profile NM-4. **C**. Interpreted seismic profile NM-4. **D.** Uninterpreted seismic profile NM-9. **E.** Interpretation of seismic profile NM-9. Both profiles show U1 seismic unit overlain by downlapping U2 seismic unit interpreted as external slope deposits derived from the quaternary barrier reef.

Figure 7: A. 3D bathymetrical map of the outer slope in front of Côte Oubliée with location of seismic profiles NM-12B and NM-13 and dredged carbonate rock DR-49 (see Table 3). **B.** Uninterpreted seismic profile NM-12B. **C.** Interpretation of seismic profile NM-12B. **D.** Uninterpreted seismic profile NM-13. **E**. Interpretation of seismic profile NM-13. The upper slope is characterized by a thick downlapping U1 sedimentary unit incised by numerous gullies suggesting significant off-bank transport from the lagoon towards the basin.

Figure 8: A. 3D bathymetrical map of the southeastern slope of Grande Terre and Pines Ridge with location of AUS-104 and 206-04 seismic profiles. T : Banc de la Torche ; S : Stylaster seamount ; B : Brachiopod seamount ; A : Antigonia seamount ; C : Crypthelia seamount ; M : Munida seamount. **B.** Seismic profile AUS-14 across the Loyalty Basin bordered by the Loyalty and Pines ridges. **C.** Line drawing interpretation of profile AUS-14 showing spectacular normal faults affecting the peridotite nappe overlain by post-obduction sedimentary units. This study focuses on shallow-water carbonates that cover peridotite horsts of the Pines Ridge and which are currently at 300-400 m water depths.

Figure 9: Bathymetric map (**A**) and profile (**B**) of Crypthelia seamount located from 200 to 800 m water depth and marked by N160° oriented faults (f) associated with a channel (Ch) and large collapses on its southern edge. Bathymetric map of Munida seamount (**C**) marked by a southern terrace noted M1, located between 400 to 600 m water depth, and by a relatively flat top above 200 m water depth, noted M2.

Figure 10: A. Seismic profile 206-04 through the Pines Ridge and Munida seamount (see location on Fig.8A and 10C). **B.** Interpretation of profile 206-04 showing the normally faulted geometry the Peridotite Nappe and HP-LT Metamorphic complex resulting from post-obduction extensional tectonics (Patriat et al., 2018). Associated flat-topped horsts are capped by a shallow water carbonate ramp interpreted as being of Mio-Pliocene age based on biostratigraphic analysis of DW-4757 and DW-4782-A dredged samples (see Table 3). **C**. Close-up view on seismic profile 206-04 on the Pines Ridge. **D**. Detailed line drawing interpretation of C. showing

3 subunits UP1 to UP3 and an overall asymmetric configuration suggesting a tilt of Pines Ridge before and during deposition of the Mio-Pliocene carbonate ramp. The eastern part of UP2 subunit is characterized by buid-up geometries that could be interpreted as aggrading platform.

Figure 11: A. DR44 sample, (a.) *Katacycloclypeus martini*, (b.) *Globigerinoides quadrilobatus*. **B.** DR44 sample, (a.) *small rotaliid* in reworked micrite, (b.) *Dentoglobigerina altispira*, (c.) *Globorotalia menardii*, (d.) *Globigerinoides conglobatus*, (e.) *Globigerinoides ruber*. **C.** DR44 sample, (a.) *Globorotalia plesiotumida*. **D.** DR45 sample, (a.) *Lepidocyclina sp..* **E.** DR46 sample, (a.) *Truncorotalia crassaformis.* **F.** DR47 sample, (a.) *Globoquadrina dehiscens.* G. DR47 sample, (a.) *Globorotalia tumida.*

Figure 12: A. DR48 sample, (a.) *Alveolinella praequoyi* (b.) *Pulleniatina obliquiloculata.* **B.** DR49 sample, (a.) *Alveolinella praequoyi*. **C.** DR49 sample, (a.) *Globorotalia tumida* **D.** DR53 sample, (a.) *Pulleniatina primalis* **E.** DW4737-B sample, (a.) *Alanlordia sp.* **F.** DW4757-A sample, (a.) *Planorbulinella solida.* **G.** DW4770 sample, (a.) *Truncorotalia truncatulinoides* (d'Orbigny) (b.) *Truncorotalia tosaensis* (Takayanagi and Saito).

Figure 13: A. Schematic cross-sections showing the geometry and evolution of shallow water post-obduction systems on the eastern margin of Grande Terre in the vicinity of Poindimié (1), north of Pines Ridges along Banc de la Torche (2), south of Pines Ridge (3), and over Crypthelia (4) and (5)Munida seamounts. (location in Fig. 13C). **B.** Paleogeographical reconstruction and spatial distribution of Mio-Pliocene carbonate banks. **C.** Paleogeographical reconstruction and spatial distribution of Quaternary barrier reef of Grande Terre and submerged isolated platforms along Pines Ridges and seamounts.

Table 1: Characteristics of the seismic acquisition devices.

Table 2: List of carbonate rock samples analysed in this study

Table 3: Table summarizing microfacies description and interpretation of depositional environment, age of *in-situ* components and age of reworked components (identified in red in Table 4)

Table 4: List of the component occurrence with identification of reworked elements (red cross).

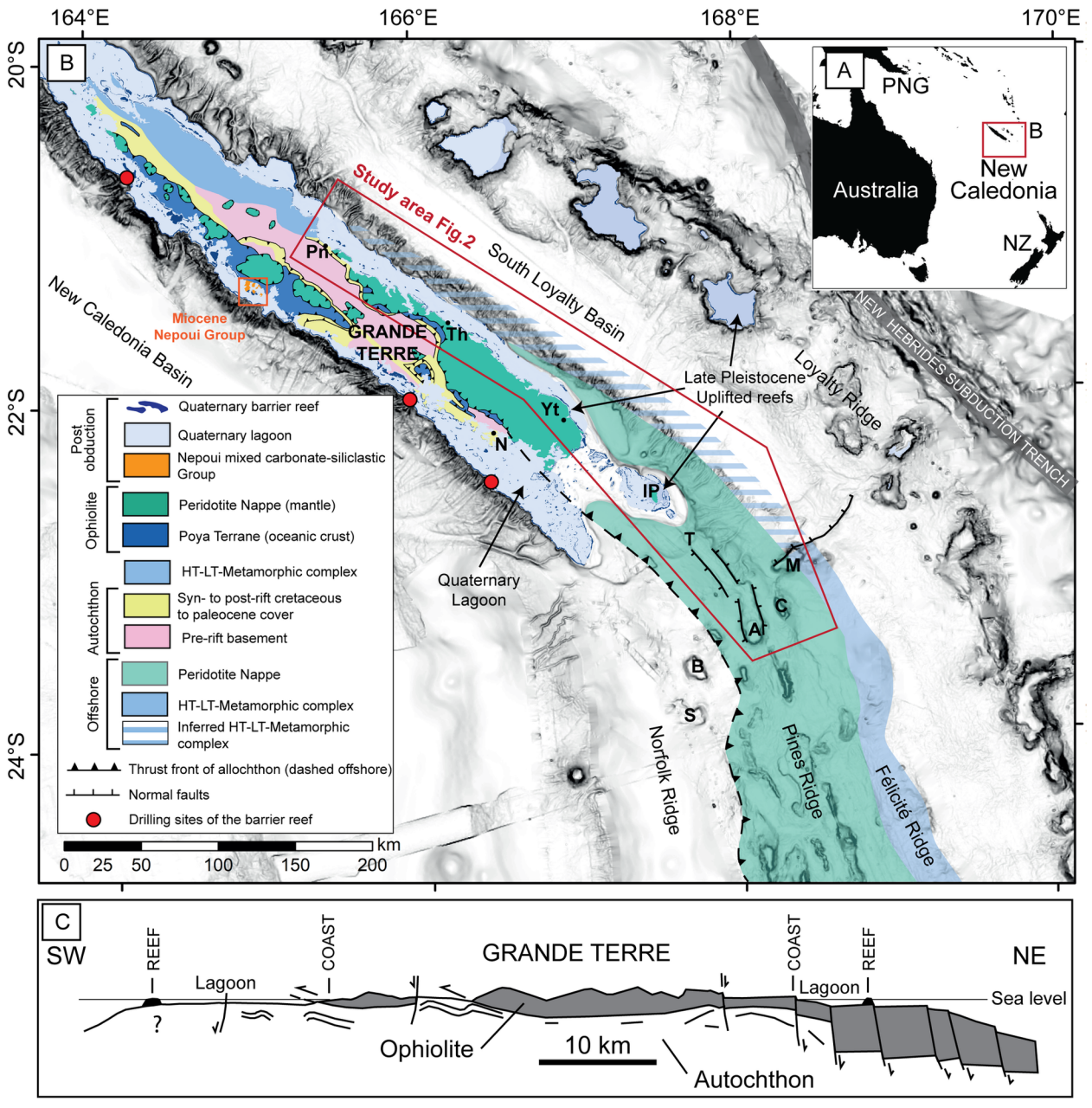
164°E
166°E
168°E
170°E
20°S
22°S
24°S
B
A
PNG
Australia
B
New Caledonia
NZ
Study area Fig.2
South Loyalty Basin
New Caledonia Basin
Miocene Nepoui Group
GRANDE TERRE
Pn
Th
Yt
N
IP
T
M
C
A
B
S
Late Pleistocene Uplifted reefs
Loyalty Ridge
NEW HEBRIDES SUBDUCTION TRENCH
Quaternary Lagoon
Norfolk Ridge
Pines Ridge
Félicité Ridge
Post obduction
Quaternary barrier reef
Quaternary lagoon
Nepoui mixed carbonate-siliclastic Group
Ophiolite
Peridotite Nappe (mantle)
Poya Terrane (oceanic crust)
HT-LT-Metamorphic complex
Autochthon
Syn- to post-rift cretaceous to paleocene cover
Pre-rift basement
Offshore
Peridotite Nappe
HT-LT-Metamorphic complex
Inferred HT-LT-Metamorphic complex
Thrust front of allochthon (dashed offshore)
Normal faults
Drilling sites of the barrier reef
km
0 25 50 100 150 200
C
SW
REEF
Lagoon
?
COAST
GRANDE TERRE
COAST
REEF
Lagoon
NE
Sea level
Ophiolite
10 km
Autochthon

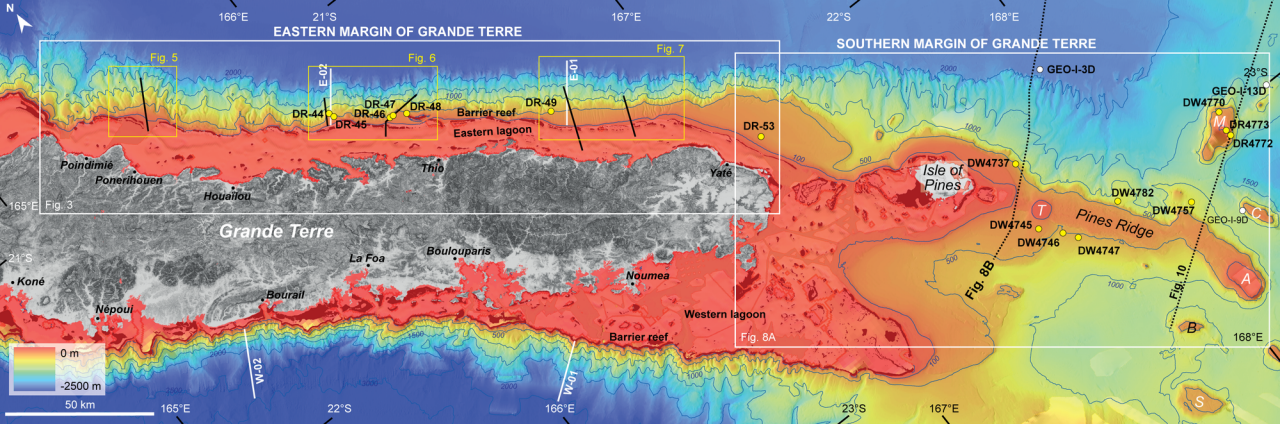
N
166°E
21°S
167°E
22°S
168°E
EASTERN MARGIN OF GRANDE TERRE
SOUTHERN MARGIN OF GRANDE TERRE
Fig. 5
Fig. 6
Fig. 7
E-02
E-01
DR-44
DR-45
DR-46
DR-47
DR-48
DR-49
Barrier reef
Eastern lagoon
DR-53
GEO-I-3D
33°S
GEO-I-13D
DW4770
M
DR4773
DR4772
Poindimié
Ponérihouen
Houaïlou
Thio
Yaté
165°E
Fig. 3
Grande Terre
DW4737
Isle of Pines
DW4782
DW4757
GEO-I-9D
C
T
Pines Ridge
DW4745
DW4746
DW4747
Fig. 8B
Fig. 10
A
B
21°S
Koné
La Foa
Boulouparis
Nouméa
Nepoui
Boulrail
Western lagoon
Barrier reef
Fig. 8A
168°E
0 m
-2500 m
50 km
W-02
W-01
165°E
22°S
166°E
23°S
167°E
S

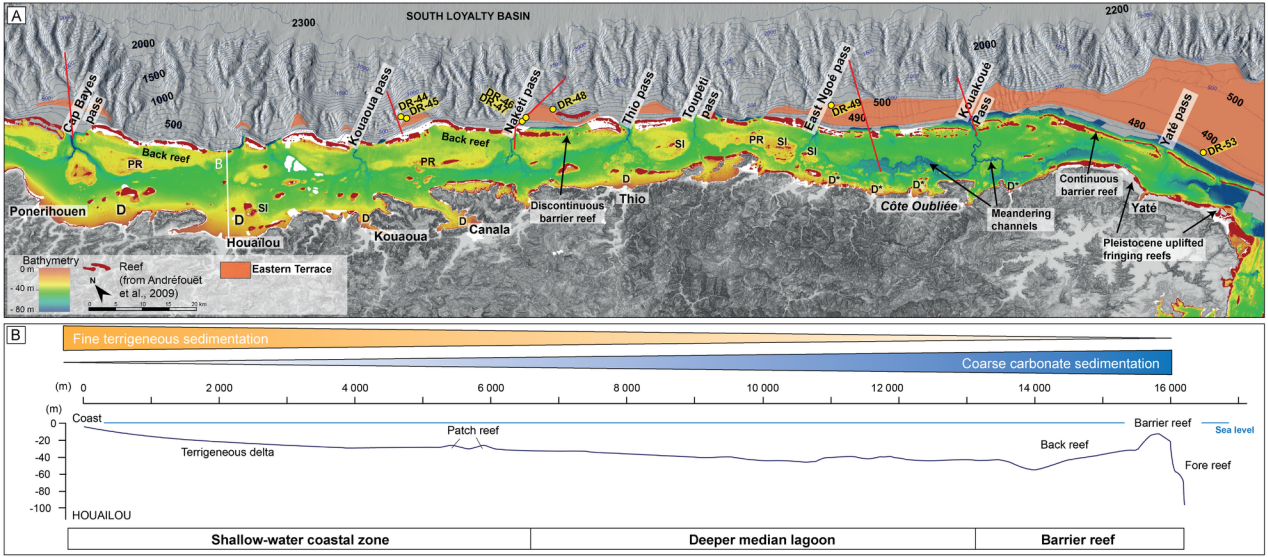
A
SOUTH LOYALTY BASIN
2300
2200
2000
1500
1000
500
Cap Bayes pass
Kouaoua pass
DR-44
DR-45
DR-47
DR-48
Nakéti pass
DR-46
Thio pass
Toupeti pass
East Ngoé pass
DR-49
500
490
Koulakoué pass
480
Yaté pass
DR-53
Back reef
PR
SI
D
D*
Ponerihouen
Houaïlou
Kouaoua
Canala
Thio
Discontinuous barrier reef
Côte Oubliée
Meandering channels
Continuous barrier reef
Yaté
Pleistocene uplifted fringing reefs
Bathymetry
0 m
- 40 m
- 80 m
Reef (from Andréfouët et al., 2009)
Eastern Terrace
B
Fine terrigeneous sedimentation
Coarse carbonate sedimentation
(m)
0
2 000
4 000
6 000
8 000
10 000
12 000
14 000
16 000
Coast
Patch reef
Barrier reef
Sea level
Terrigeneous delta
Back reef
Fore reef
-20
-40
-60
-80
-100
HOUAILOU
Shallow-water coastal zone
Deeper median lagoon
Barrier reef

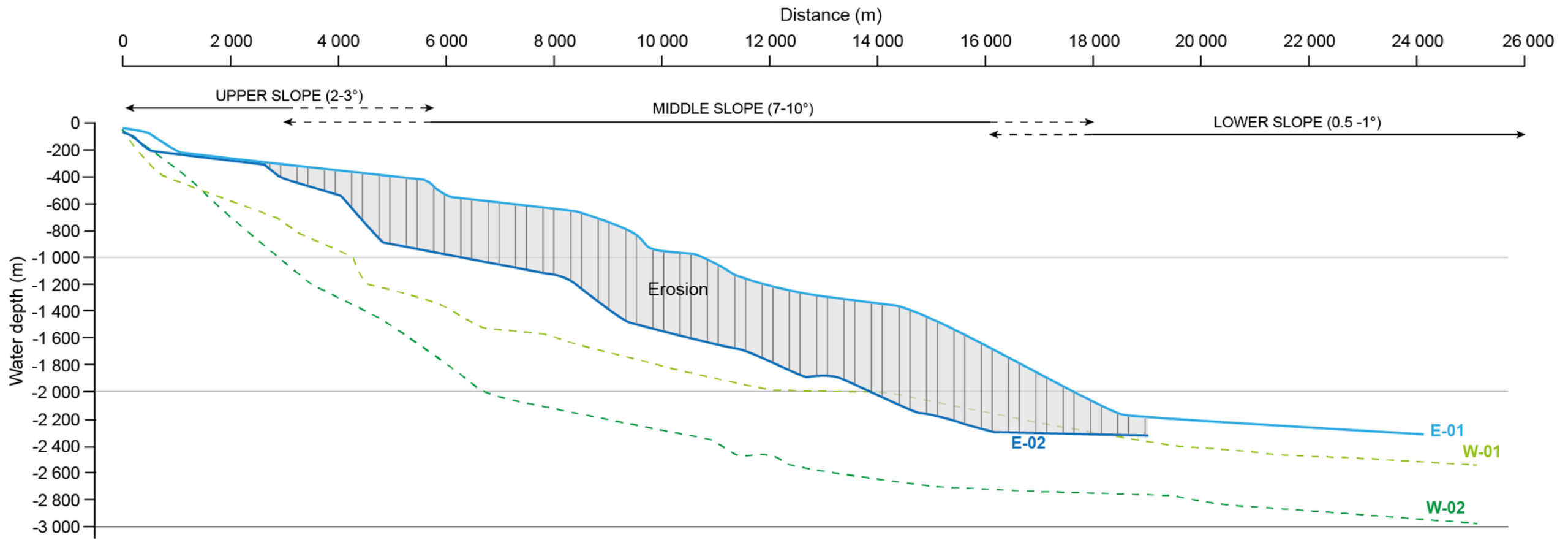
Distance (m)
0
2 000
4 000
6 000
8 000
10 000
12 000
14 000
16 000
18 000
20 000
22 000
24 000
26 000
UPPER SLOPE (2-3°)
MIDDLE SLOPE (7-10°)
LOWER SLOPE (0.5 -1°)
Water depth (m)
0
-200
-400
-600
-800
-1 000
-1 200
-1 400
-1 600
-1 800
-2 000
-2 200
-2 400
-2 600
-2 800
-3 000
Erosion
E-02
E-01
W-01
W-02

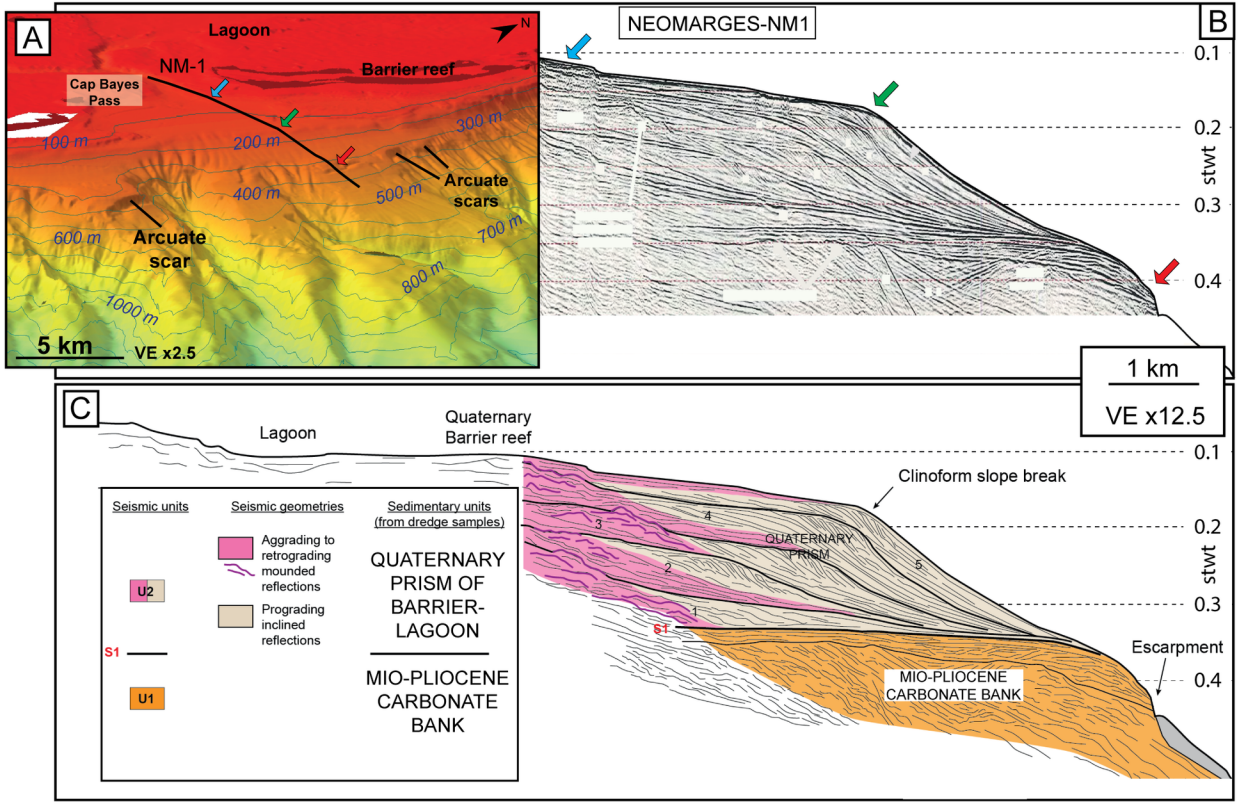
A
Lagoon
N
NM-1
Barrier reef
Cap Bayes Pass
100 m
200 m
300 m
400 m
500 m
600 m
700 m
800 m
1000 m
Arcuate scars
Arcuate scar
5 km
VE x2.5
B
NEOMARGES-NM1
0.1
0.2
0.3
0.4
stwt
1 km
VE x12.5
C
Lagoon
Quaternary Barrier reef
Clinoform slope break
Seismic units
Seismic geometries
Sedimentary units (from dredge samples)
Aggrading to retrograding mounded reflections
Prograding inclined reflections
U2
S1
U1
QUATERNARY PRISM OF BARRIER-LAGOON
MIO-PLIOCENE CARBONATE BANK
QUATERNARY PRISM
MIO-PLIOCENE CARBONATE BANK
Escarpment
1
2
3
4
5

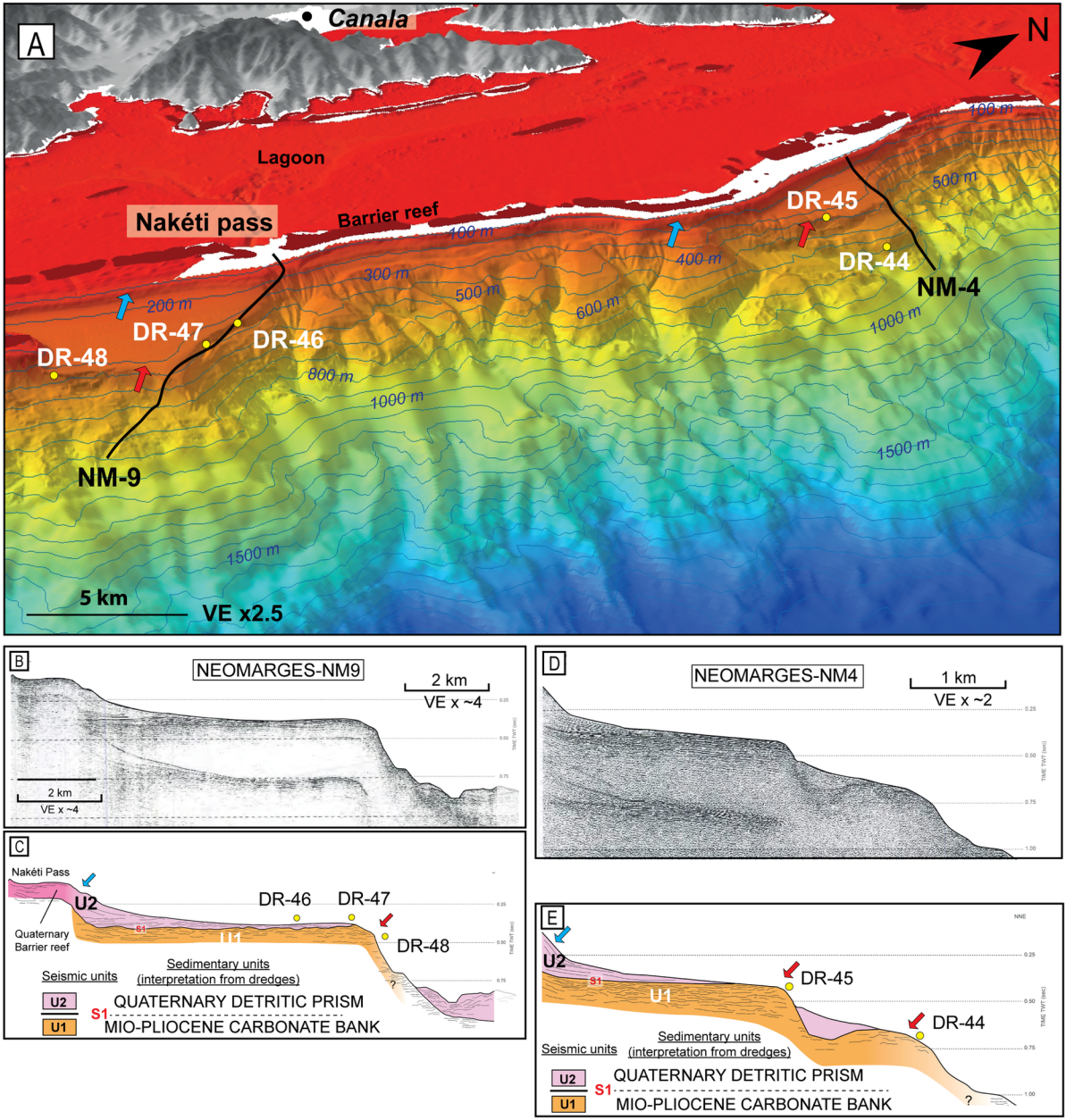
A
Canala
N
Lagoon
Nakéti pass
Barrier reef
100 m
200 m
300 m
400 m
500 m
600 m
800 m
1000 m
1500 m
DR-45
DR-44
NM-4
DR-47
DR-46
DR-48
NM-9
5 km
VE x2.5
B
NEOMARGES-NM9
2 km
VE x ~4
D
NEOMARGES-NM4
1 km
VE x ~2
C
Nakéti Pass
U2
Quaternary
Barrier reef
S1
U1
DR-46
DR-47
DR-48
Seismic units
Sedimentary units
(interpretation from dredges)
QUATERNARY DETRITIC PRISM
MIO-PLIOCENE CARBONATE BANK
E
NNE
DR-45
DR-44

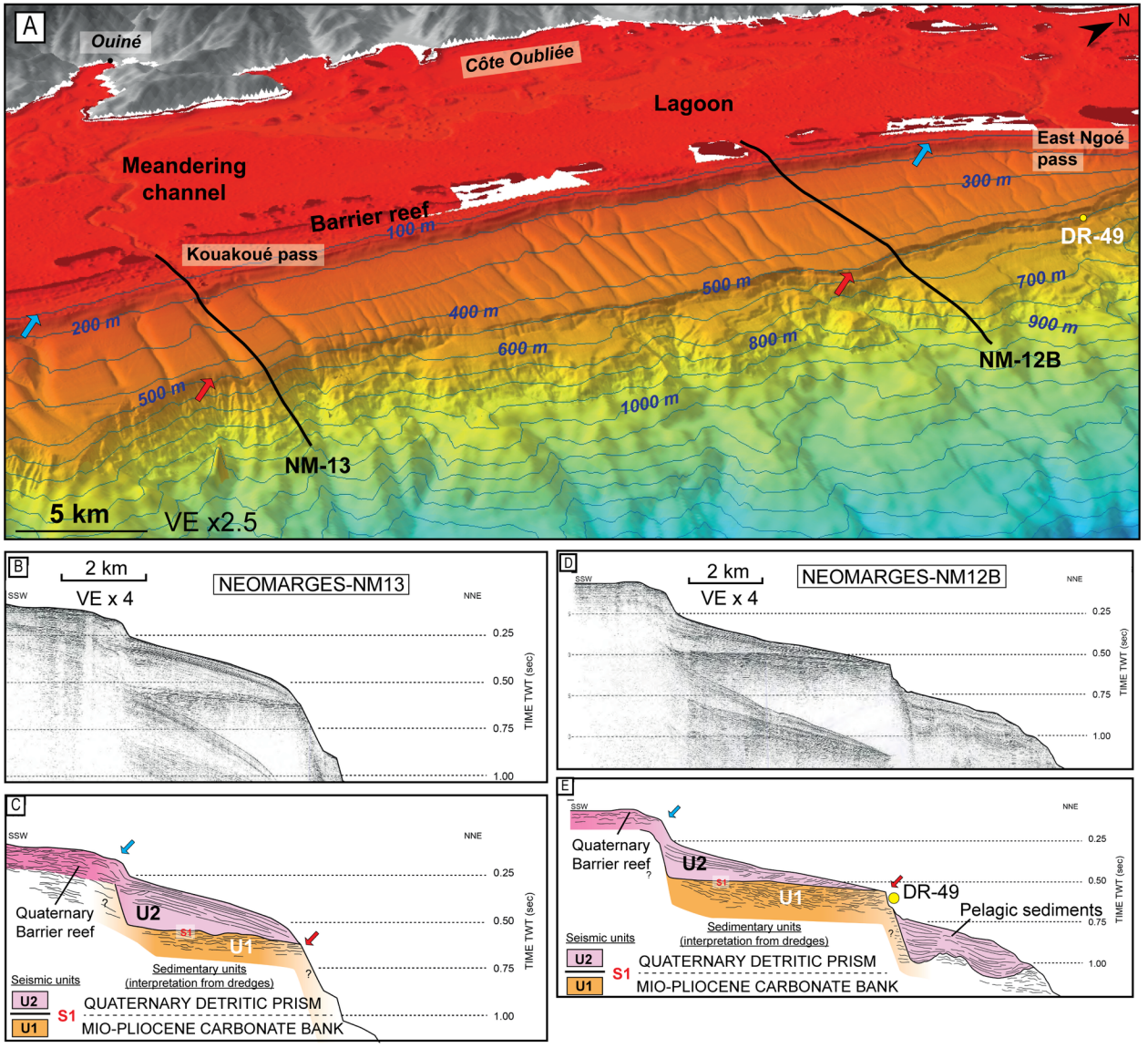
A
Ouiné
Côte Oubliée
N
Lagoon
East Ngoé pass
Meandering channel
Barrier reef
100 m
300 m
DR-49
Kouakoué pass
200 m
400 m
500 m
700 m
600 m
800 m
900 m
NM-12B
500 m
1000 m
NM-13
5 km
VE x2.5
B
2 km
VE x 4
NEOMARGES-NM13
SSW
NNE
0.25
0.50
0.75
1.00
TIME TWT (sec)
D
2 km
VE x 4
NEOMARGES-NM12B
SSW
NNE
0.25
0.50
0.75
1.00
TIME TWT (sec)
C
SSW
NNE
Quaternary Barrier reef
U2
S1
U1
Sedimentary units (interpretation from dredges)
Seismic units
U2
S1
QUATERNARY DETRITIC PRISM
U1
MIO-PLIOCENE CARBONATE BANK
0.25
0.50
0.75
1.00
TIME TWT (sec)
E
SSW
NNE
Quaternary Barrier reef
U2
S1
U1
DR-49
Pelagic sediments
Sedimentary units (interpretation from dredges)
Seismic units
U2
S1
QUATERNARY DETRITIC PRISM
U1
MIO-PLIOCENE CARBONATE BANK
0.25
0.50
0.75
1.00
TIME TWT (sec)

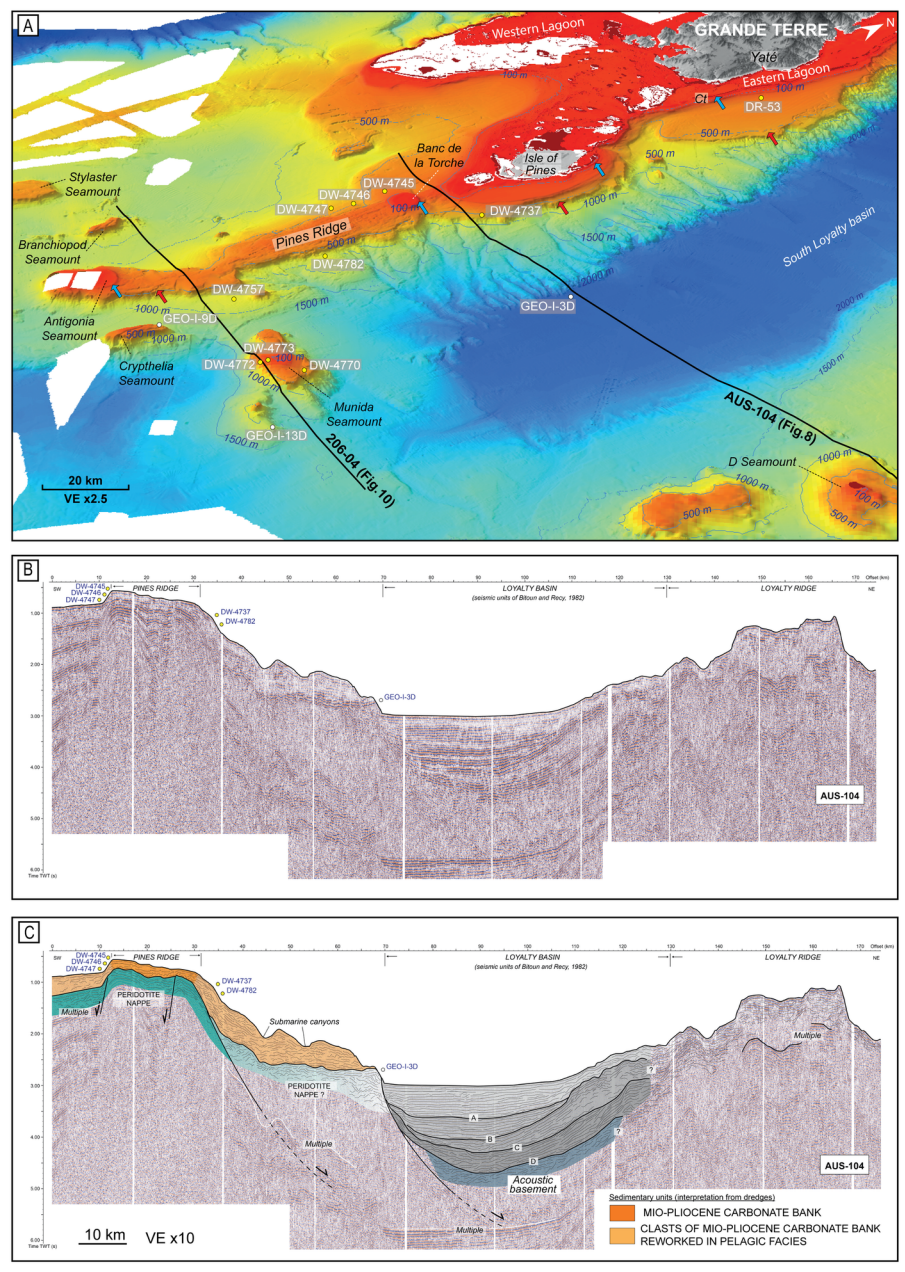
A
GRANDE TERRE
N
Western Lagoon
Yaté
Eastern Lagoon
100 m
Ct
DR-53
500 m
Banc de la Torche
Isle of Pines
Stylaster Seamount
DW-4746
DW-4745
DW-4747
DW-4737
1000 m
1500 m
Pines Ridge
Branchiopod Seamount
DW-4782
South Loyalty basin
DW-4757
GEO-I-3D
2000 m
Antigonia Seamount
GEO-I-9D
DW-4773
DW-4772
DW-4770
Crypthelia Seamount
Munida Seamount
GEO-I-13D
AUS-104 (Fig.8)
206-04 (Fig.10)
D Seamount
20 km
VE x2.5
B
SW
NE
Offset (km)
PINES RIDGE
LOYALTY BASIN
(seismic units of Bitoun and Recy, 1982)
LOYALTY RIDGE
DW-4745
DW-4746
DW-4747
DW-4737
DW-4782
GEO-I-3D
AUS-104
Time TWT (s)
C
PERIDOTITE NAPPE
Multiple
Submarine canyons
PERIDOTITE NAPPE ?
A
B
C
D
Acoustic basement
10 km
VE x10
Sedimentary units (interpretation from dredges)
MIO-PLIOCENE CARBONATE BANK
CLASTS OF MIO-PLIOCENE CARBONATE BANK REWORKED IN PELAGIC FACIES

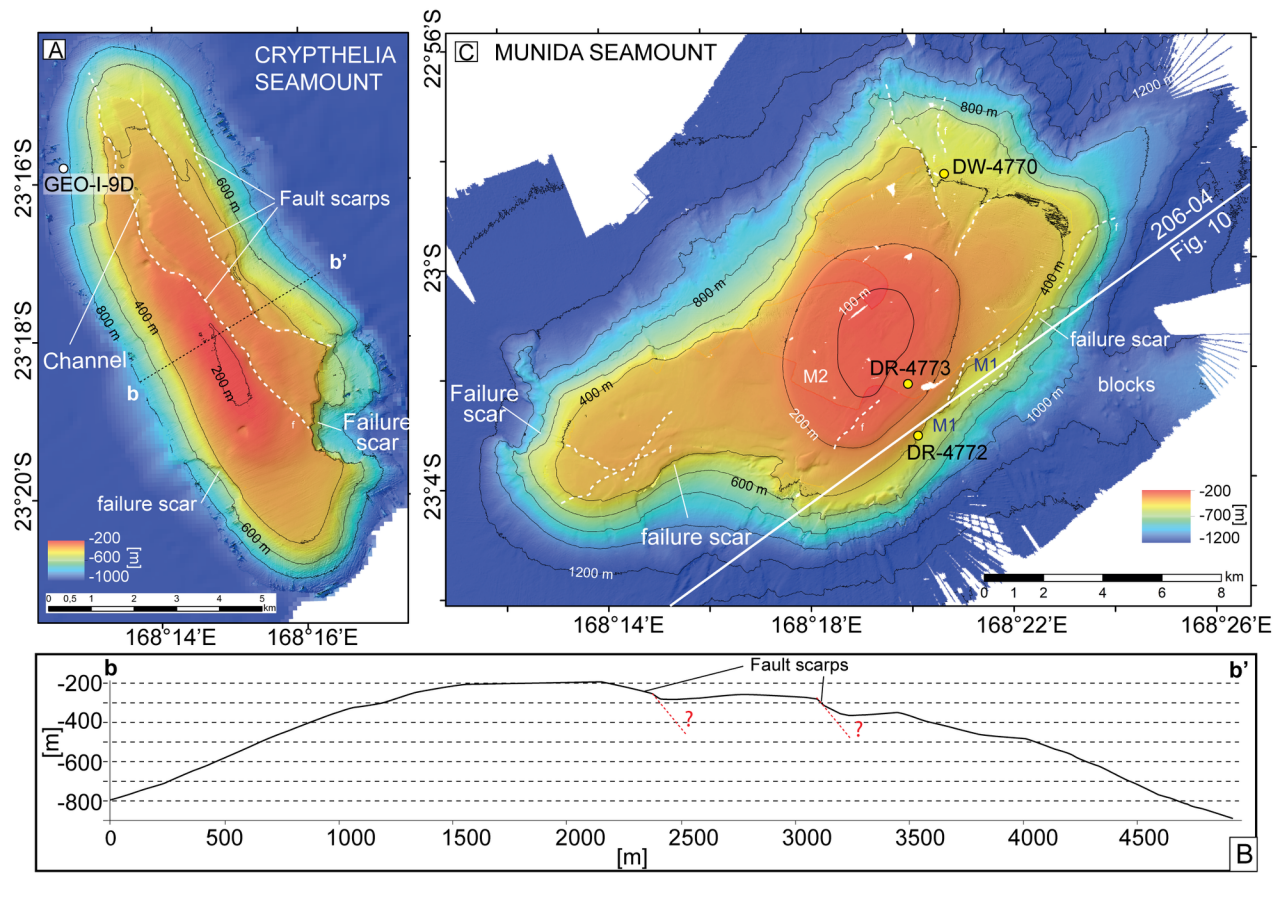
A
CRYPTHELIA SEAMOUNT
GEO-I-9D
Fault scarps
b'
b
Channel
600 m
400 m
200 m
Failure scar
failure scar
-200
-600
-1000
m
0 0,5 1 2 3 4 5 km
23°16'S
23°18'S
23°20'S
168°14'E
168°16'E
C
MUNIDA SEAMOUNT
22°56'S
23°S
23°4'S
DW-4770
800 m
1200 m
206-04
Fig. 10
400 m
M2
DR-4773
M1
failure scar
blocks
Failure scar
200 m
1000 m
M1
DR-4772
600 m
failure scar
1200 m
-200
-700
-1200
m
0 1 2 4 6 8 km
168°14'E
168°18'E
168°22'E
168°26'E
b
b'
Fault scarps
-200
-400
-600
-800
[m]
?
?
0
500
1000
1500
2000
2500
3000
3500
4000
4500
[m]
B

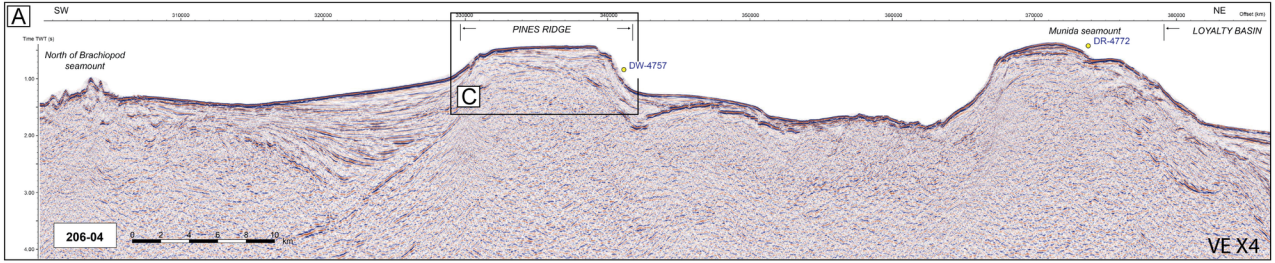
A
SW
NE
Offset (km)
Time TWT (s)
PINES RIDGE
North of Brachiopod seamount
DW-4757
Munida seamount
DR-4772
LOYALTY BASIN
C
206-04
VE X4

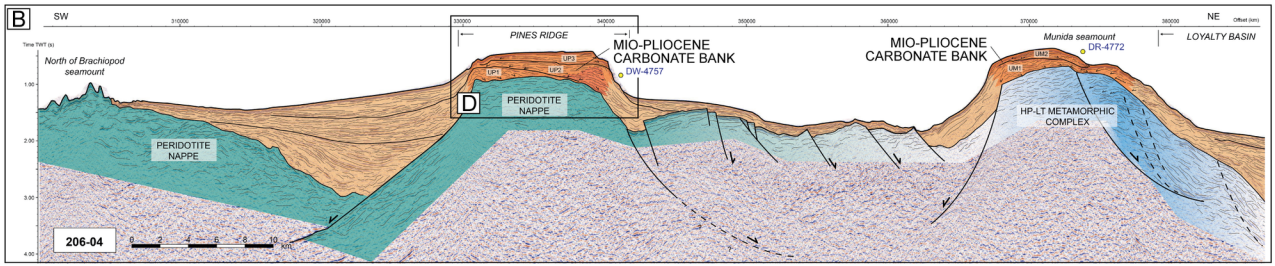
B
SW
NE
Offset (km)
Time TWT (s)
PINES RIDGE
North of Brachiopod seamount
MIO-PLIOCENE CARBONATE BANK
DW-4757
Munida seamount
DR-4772
MIO-PLIOCENE CARBONATE BANK
LOYALTY BASIN
UP1
UP2
UP3
UM1
UM2
D
PERIDOTITE NAPPE
PERIDOTITE NAPPE
HP-LT METAMORPHIC COMPLEX
206-04

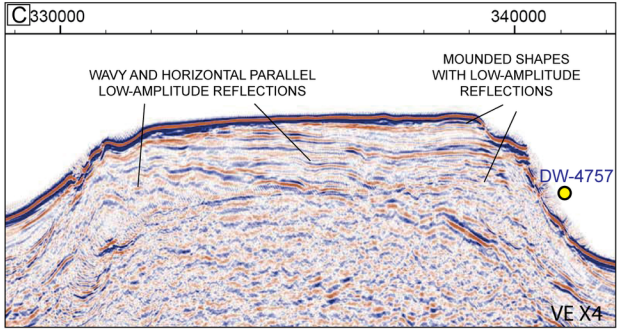
C
330000
340000
WAVY AND HORIZONTAL PARALLEL LOW-AMPLITUDE REFLECTIONS
MOUNDED SHAPES WITH LOW-AMPLITUDE REFLECTIONS
DW-4757
VE X4

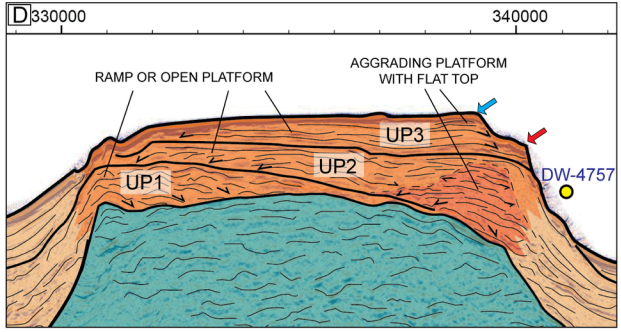
D
330000
340000
RAMP OR OPEN PLATFORM
AGGRADING PLATFORM WITH FLAT TOP
UP1
UP2
UP3
DW-4757

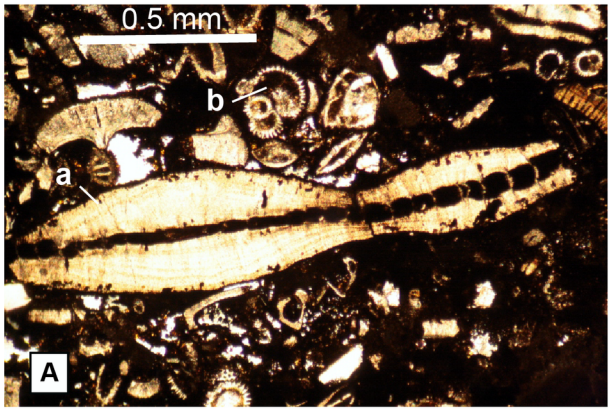
0.5 mm
b
a
A

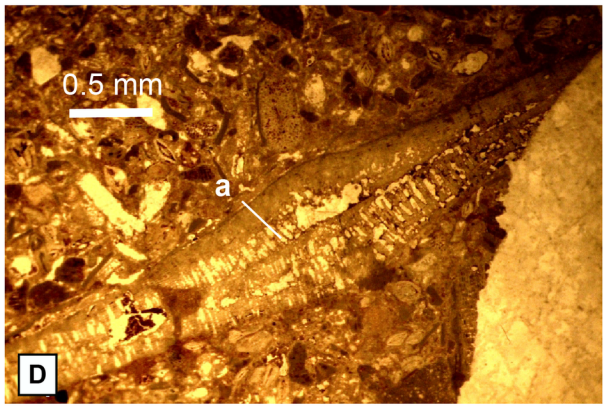
0.5 mm
a
D

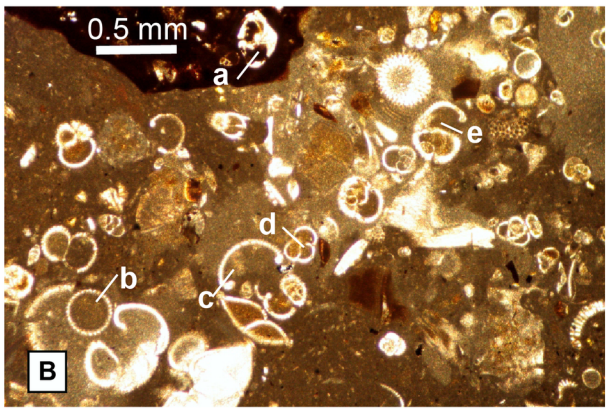
0.5 mm
a
e
d
b
c
B

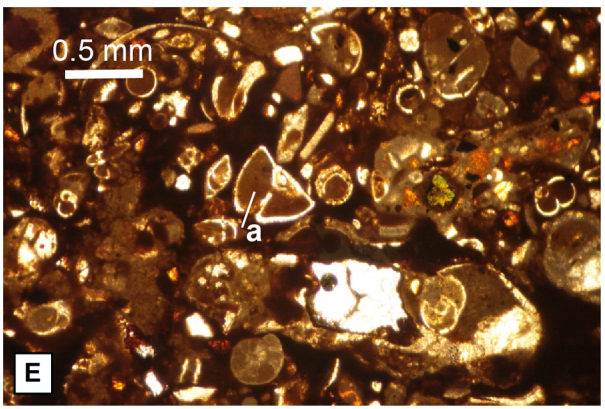
0.5 mm
a
E

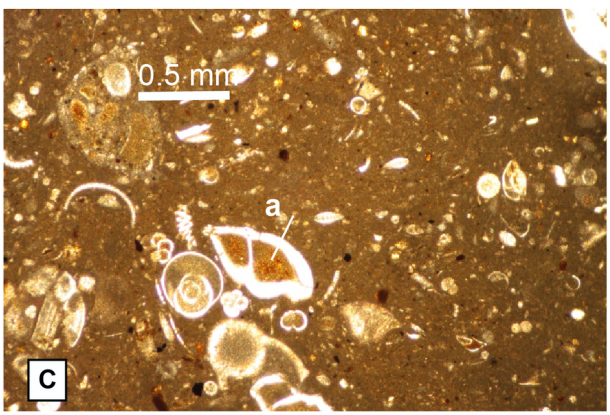
0.5 mm
a
C


0.5 mm
a
F


0.5 mm
a
G

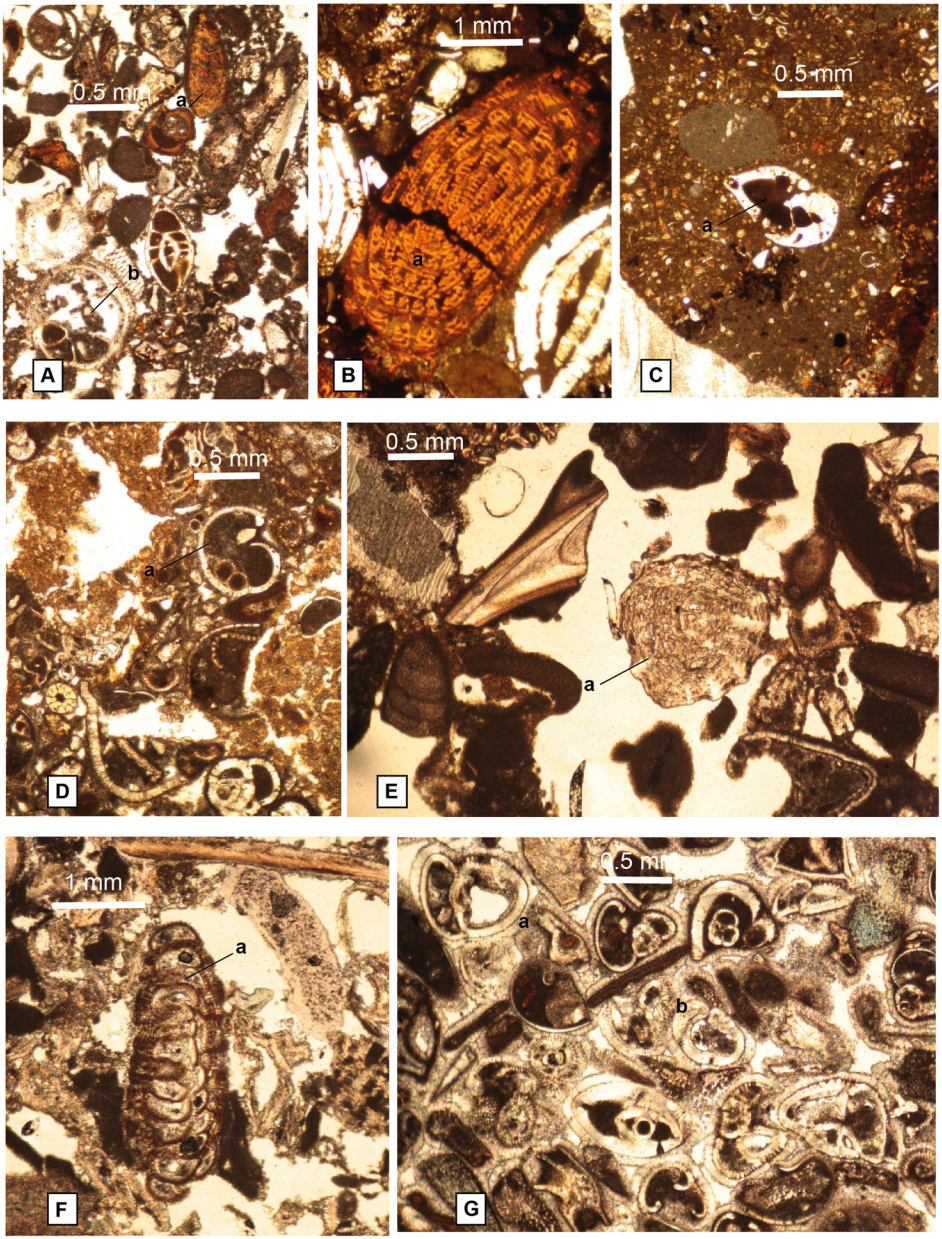
0.5 mm
a
b
A
1 mm
a
B
0.5 mm
a
C
0.5 mm
a
D
0.5 mm
a
E
1 mm
a
F
0.5 mm
a
b
G

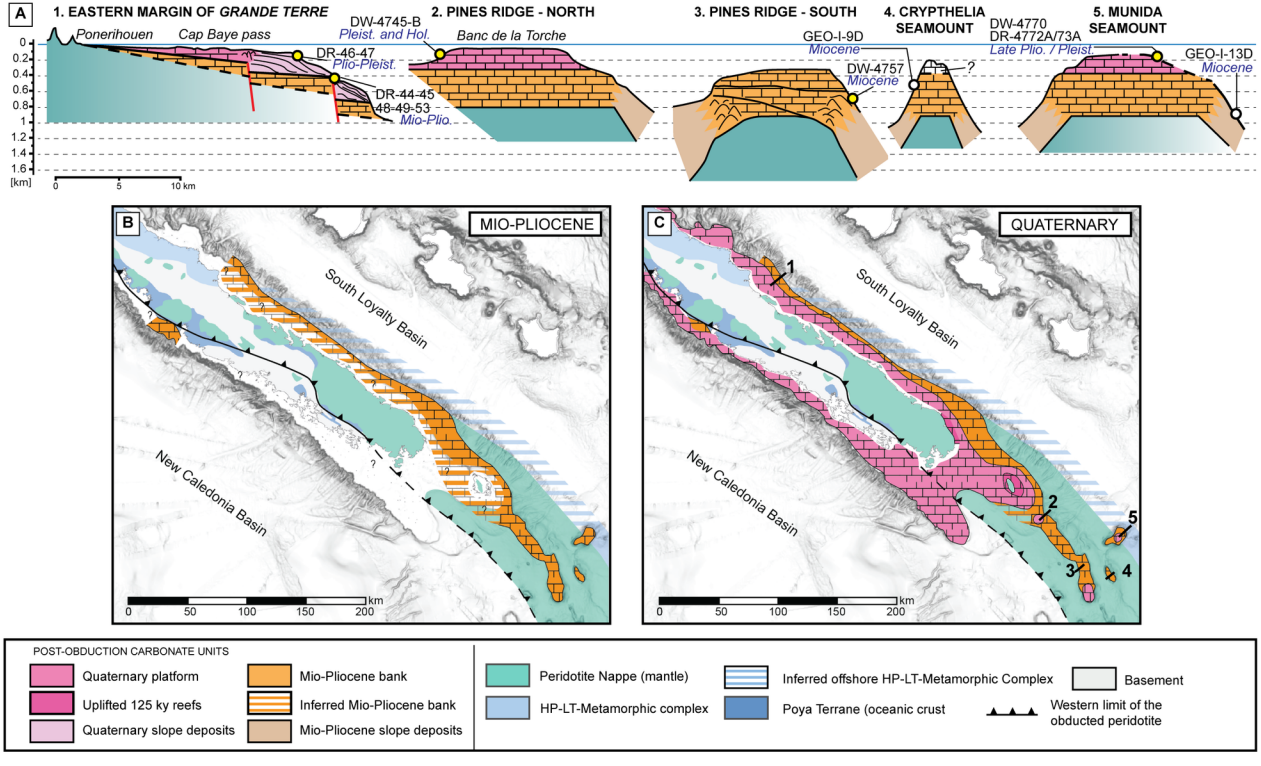
A
1. EASTERN MARGIN OF GRANDE TERRE
Ponerihouen
Cap Baye pass
DW-4745-B
Pleist. and Hol.
DR-46-47
Plio-Pleist.
DR-44-45
48-49-53
Mio-Plio.
2. PINES RIDGE - NORTH
Banc de la Torche
3. PINES RIDGE - SOUTH
GEO-I-9D
Miocene
DW-4757
Miocene
4. CRYPTHELIA SEAMOUNT
?
DW-4770
DR-4772A/73A
Late Plio. / Pleist.
5. MUNIDA SEAMOUNT
GEO-I-13D
Miocene
0
0.2
0.4
0.6
0.8
1
1.2
1.4
1.6
[km]
0
5
10 km
B
MIO-PLIOCENE
South Loyalty Basin
New Caledonia Basin
km
0
50
100
150
200
C
QUATERNARY
South Loyalty Basin
New Caledonia Basin
1
2
3
4
5
km
0
50
100
150
200
POST-OBDUCTION CARBONATE UNITS
Quaternary platform
Uplifted 125 ky reefs
Quaternary slope deposits
Mio-Pliocene bank
Inferred Mio-Pliocene bank
Mio-Pliocene slope deposits
Peridotite Nappe (mantle)
HP-LT-Metamorphic complex
Inferred offshore HP-LT-Metamorphic Complex
Poya Terrane (oceanic crust
Basement
Western limit of the obducted peridotite

SEISMIC PROFILE	***Figure in this study***	**CRUISE**	**STREAMER LENGHT (KM)**	**NUMBER OF CHANNELS**	**SOURCE TYPE**	**SOURCE VOLUME (CU)**	**SOURCE BAND WIDTH (Hz)**	**SHOT INTERVAL (m)**
NM-1	Fig. 5	NEOMARGES, 2006	0.072	24	Airgun Bolt 600BT	20	50 to 500	5,5 to 8
NM-4	Fig. 6B							
NM-9	Fig. 6C							
NM-12B	Fig. 7B							
NM-13	Fig. 7C							
AUS-104	Fig. 8B	AUSTRADEC-1, 1972	_	12 or 24	Flexichoc source	_	_	_
206-04	Fig. 10	FAUST-1, 1998	3.3	264	Systems HG Sleeve guns	3000	50-60	50

SAMPLE NAME	CRUISE	SITE	WATER DEPTH (m)	LATITUDE	LONGITUDE
DR44	2005-NC-DR	Eastern margin of *Grande Terre*	550 to 680	-21.276	166.020
DR45	2005-NC-DR	Eastern margin of *Grande Terre*	300 to 410	-21.295	166.023
DR46	2005-NC-DR	Eastern margin of *Grande Terre*	295 to 380	-21.404	166.170
DR47	2005-NC-DR	Eastern margin of *Grande Terre*	295 to 380	-21.405	166.183
DR48	2005-NC-DR	Eastern margin of *Grande Terre*	290 to 400	-21.426	166.220
DR49	2005-NC-DR	Eastern margin of *Grande Terre*	400 to 500	-21.701	166.598
DR53	2005-NC-DR	Eastern margin of *Grande Terre*	280	-22.168	167.092
DW4737-B	KANACONO	Southern margin of Isle of Pines	387 to 456	-22.716	167.709
DW4746-B	KANACONO	Southern margin of Isle of Pines	494 to 508	-22.975	167.693
DW4745-B	KANACONO	Southern margin of Isle of Pines	310 to 403	-22.918	167.636
DW4747-B1	KANACONO	Southern margin of Isle of Pines	550 to 590	-23.015	167.722
DW4747-X	KANACONO	Southern margin of Isle of Pines	550 to 590	-23.015	167.722
DW4757-A	KANACONO	Southern margin of Isle of Pines	800 to 850	-23.142	168.096
DW4782-A	KANACONO	Southern margin of Isle of Pines	845 to 856	-23.000	167.903
DW4770	KANACONO	Munida seamount	455 to 470	-22.975	168.350
DR4772-A	KANACONO	Munida seamount	230 to 795	-23.051	168.336
DR4773-A	KANACONO	Munida seamount	230 to 400	-23.035	168.334

SAMPLES	SITE	DEPTH	CRUISE	MICROFACIES	DEPOSITIONAL ENVIRONNEMENT	ZONE and AGE	ZONE and AGE of reworked components (in red Table.4)
DR44	Eastern Margin, in front of Canala (Fig.6)	550 to 680 m	2005-NC-DR	Micritic pelagic packstone with reworked micritic patches of planktonic foraminifera, recrystallised algae and larger benthic foraminifera	Forereef environment LBF reworked into inner to outer neritic environment	N19-N20a (5.3 Ma to 3.6 Ma) Early Pliocene	N12 (13.82 Ma to 12.00 Ma) Serravallian
DR45		300 to 410 m	2005-NC-DR	Micritic pelagic packstone with reworked micritic patches of planktonic foraminifera, recrystallised algae and larger benthic foraminifera	Forereef environment LBF reworked into inner to outer neritic environment	N19-N20a (5.33 Ma to 3.6 Ma) Early Pliocene	N12-N13 (13.82 Ma to 11.63 Ma) Serravallian
DR46	Eastern Margin, in front of Nakéti Pass (Fig.6)	295 to 380 m	2005-NC-DR	Micritic packstone of planktonic foraminifera with reworked patches of reworked pelagic micrite	Inner to outer neritic	N22a (1.8 Ma to 1.00 Ma) Pleistocene	N4-N17a (23.03-7.2Ma) Miocene
DR47		295 to 380 m	2005-NC-DR	Micritic wackestone of recrystallised algae with reworked patches of reworked pelagic micrite	Inner to outer neritic	N20a (3.8 Ma-3.6 Ma) Late Pliocene	N4-N17a (23.03-7.2Ma) Miocene
DR48		290 to 400 m	2005-NC-DR	Micritic packstone of algae with reworked patches of reworked pelagic micrite	Forereef environment LBF reworked into inner to outer neritic environment	N22 (1.8 Ma to 0.12 Ma) Pleistocene	N12-N13 (13.82 Ma to 11.63 Ma) Serravallian
DR49	Eastern Margin, in front of Ngoé Pass (Fig.7)	400 to 500 m	2005-NC-DR	Micritic packstone of algae and larger benthic foraminifera reworked into pelagic micrite	Forereef environment LBF reworked into inner to outer neritic environment	N19 (5.3 Ma to 3.8 Ma) Early Pliocene	N12-N13 (13.82 Ma to 11.63 Ma) Serravallian
DR53	Eastern Margin, in front of Yaté (Fig.8)	280 m	2005-NC-DR	Micritic packstone of planktonic foraminifera	Inner to outer neritic	N18-N21a (5.8 Ma to 2.5 Ma) Late Miocene (Messinian) to Early Pliocene (Zanclean))	Serravallian to Pliocene, N12-N21
DW4737-B	SE Isle of Pines (Fig.8)	387 to 456 m	KANACONO	Micritic wackestone of foraminifera and fragments of algae	Inner to outer neritic	N20b-N21 (3.6 Ma to 2.5 Ma) Pliocene	
DW4745-B	West of Pines Ridge (Fig.8)	310 to 403 m	KANACONO	Micritic packsotne of foraminifera and algae	Inner to outer neritic	N22-Recent (1.8 Ma to Recent) Pleistocene - Holocene	
DW4746-B		494 to 508 m	KANACONO	Grainstone cemented by sparite of planktonic foraminifera with reworked micritic patches	Inner to outer neritic	N22 (1.8 Ma to 0.12 Ma) Pleistocene	N19-N21 (5.33 Ma to 1.8 Ma) Pliocene
DW4747-B1		550 to 590 m	KANACONO	Micritic packsotne of foraminifera and algae	Inner to outer neritic	N19-N22 (5.33 Ma to 0.12 Ma) Pliocene - Pleistocene	
DW4747-X		550 to 590 m	KANACONO	Micritic wackestone of foraminifera	Inner to outer neritic	N21-N22 (2.5 Ma to 0.12 Ma) Late Pliocene - Pleistocene	
DW4757-A	East of Pines Ridges (Fig.8)	800 to 850 m	KANACONO	Micritic wackestone of foraminifera	Forereef environment	N4-N12 (23.03 Ma to 12 Ma) Early Miocene	
DW4782-A		845 to 856 m	KANACONO	Micritic wackestone of foraminifera	Inner to outer neritic	N17-N20 (8.6 Ma to 3.4 Ma) Late Miocene - Early Pliocene	
DW4770	Munida seamount (Fig.8 and Fig.9)	455 to 470 m	KANACONO	Micritic/sparitic packstone of foraminifera and algae	Inner to outer neritic	N22 (1.8 Ma to 0.12 Ma) Pleistocene	
DR4772-A		320 to 795 m	KANACONO	Grainstone cemented by sparite of planktonic foraminifera with reworked micritic patches	Inner to outer neritic	N21-N22 (3.4 Ma to 0.12 Ma) Late Pliocene - Pleistocene	N4-N17a Miocene
DR4773-A		230 to 400 m	KANACONO	Grainstone cemented by sparite of planktonic foraminifera with reworked micritic patches	Inner to outer neritic	N21-N22 (3.4 Ma to 0.2 Ma) Late Pliocene - Pleistocene	N4-N17a (23.03-7.2Ma) Miocene

	Planktonic foraminiferra																																								
	Beella sp.	Catapsydrax cf. dissimilis	Catapsydrax sp.	Dentoglogigerina altispira	Globoquadrina dediscens	Globoquadrina sp.	Globorotalia plesiotumida	Globorotalia tumida	Globorotalia menardii	Globorotalia inflata	Globorotalia scitula	Globorotalia miocenica	Globorotalia ungulata	Globorotalia sp.	Globigerina bulloides	Globigerina praebulloides	Globigerina spp	Globigerinoides quadrilobatus	Globigerinoides conglobatus	Globigerinoides ruber	Globigerinoides trilobus	Globigerinoides obliquus	Globigerinoides spp.	Neogloboquadrina pachyderma	Neogloboquadrina humerosa	Neogloboquadrina dutertrei	Neogloboquadrina acostaensis	Neogloboguadrina spp.	Orbulina universa	Prosphaeroidinella parkerae	Pulleniatina obliquiloculata	Pulleniatina primalis	Pulleniatina praecursor	Pulleniatina sp.	Sphaeroidinella dehiscens	Sphaeroidinellopsis subdehiscens	Sphaeroidinellopsis paenedehiscens	Sphaeroidinellopsis seminulina	Truncorotalia crassaformis	Truncorotalia truncatulinoides	Truncorotalia crassula	Truncorotalia tosaensis
DR44				x	x	x	x	x	x	x								x	x	x			x						x						x		x		x			
DR45					x			x									x	x										x										x				
DR46		x						x	x	x						x		x						x	x	x			x	x									x	x		
DR47					x			x		x	x					x	x	x		x	x		x	x				x	x		x			x								
DR48																		x			x		x	x		x		x	x		x	x			x							
DR49								x	x	x				x				x			x		x													x						
DR53								x	x	x					x			x				x		x			x		x	x		x	x						x			
DW4737-B												x								x			x			x															x	
DW4745-B													x					x					x								x			x						x		
DW4746-B	x				x		x	x		x								x			x		x	x							x		x		x					x		x
DW4747-B1														x				x			x								x				x									
DW4747-X																																										x
DW4757-A																																										
DW4782-A			x															x					x		x				x							x		x				
DW4770						x												x					x			x					x									x		x
DR4772-A										x						x					x																					x
DR4773-A										x						x	x						x		x						x				x	x						x

	Benthic Foraminifera																													
	Acervulina sp.	Alanlordia sp.,	Alveolinella praequoyi	Alveolinella sp.	Amphistegina tuberculata	Amphistegina lessonii	Amphistegina spp	Baculogypsina sp.	Bolivina sp.	Brizalina sp.	Carpenteria sp.	Cycloclypeus spp.	Dasyclad spp.	Elphidium sp	Gypsina sp.	Homotrema sp	Katacycloclypeus martini	Quasirotalia guamensis	Lepidocyclina sp.	Lenticulina sp.	Marginopora sp.	Small miliolids	Nodosaria sp.	Operculina spp.	Operculinoides spp.	Paragloborotalia kugleri	Planorbulinella larvata	Planorbulinella solida	Planorbulina sp.	Sphaerogypsina sp.	Textularia sp.
DR44	x						x		x			x		x			x		x											x	
DR45			x	x			x			x									x					x					x		
DR46							x		x		x									x		x		x			x				
DR47							x		x											x		x	x								x
DR48	x		x		x				x		x		x							x	x	x	x				x				x
DR49			x			x								x	x, x				x			x			x		x				
DR53	x	x					x	x	x													x								x	
DW4737-B		x					x											x			x										
DW4745-B							x																								
DW4746-B																		x			x										
DW4747-B1											x		x							x				x					x	x	
DW4747-X							x				x																				
DW4757-A						x													x									x			
DW4782-A									x															x							
DW4770																				x											
DR4772-A																										x					
DR4773-A							x							x		x					x	x		x						x	x

	Other component							
	Radiolaria sp.,	Gastropod spp.	Rodophyte spp.	Halimeda sp.	Echinoid spp.	Bryozoa spp.	Ostracod sp.	Coral spp.
DR44	x	x	x			x		x
DR45		x	x		x			
DR46		x			x		x	
DR47	x	x	x		x			x
DR48		x	x	x	x			x
DR49		x	x		x			
DR53		x	x		x			
DW4737-B		x	x		x			x
DW4745-B			x		x			
DW4746-B			x		x			
DW4747-B1		x	x		x	x		x
DW4747-X					x			x
DW4757-A			x		x			x
DW4782-A								
DW4770			x		x			
DR4772-A			x		x			
DR4773-A		x			x			